A NUMERICAL INVESTIGATION WITH SENSITIVITY ANALYSIS OF HEAT TRANSFER PERFORMANCE IN A HEAT EXCHANGER CONTAINING NANOFLUIDS

by

Saiful Islam

Student ID: 0419093002P
Registration No.: 0419093002P
Session: April-2019

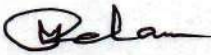**MASTER OF PHILOSOPHY**
IN
MATHEMATICS

Department of Mathematics

Bangladesh University of Engineering and Technology (BUET)
Dhaka-1000

April, 2023

The thesis entitled "**A NUMERICAL INVESTIGATION WITH SENSITIVITY ANALYSIS OF HEAT TRANSFER PERFORMANCE IN A HEAT EXCHANGER CONTAINING NANOFLUIDS**" submitted by Saiful Islam, Student ID: 0419093002P, Registration No.: 0419093002P, Session: April-2019, a part-time student of the Master of Philosophy (M.Phil.) in the department of Mathematics has been accepted as satisfactory in partial fulfillment for the degree of Master of Philosophy (M.Phil.) in Mathematics on 16th April 2023.

BOARD OF EXAMINERS

1. _____
   Dr. Md. Mustafizur Rahman
   Professor
   Dept. of Mathematics
   BUET, Dhaka-1000

   Chairman
   (Supervisor)

2. _____
   Dr. Nazma Parveen
   Professor & Head
   Dept. of Mathematics
   BUET, Dhaka-1000

   Member
   (Ex-Officio)

3. _____
   Dr. Md. Manirul Alam Sarker
   Professor
   Dept. of Mathematics
   BUET, Dhaka-1000

   Member

4. _____
   Dr. Nazma Parveen
   Professor
   Dept. of Mathematics
   BUET, Dhaka-1000

   Member

5. _____
   Dr. Md. Mamun Molla
   Professor
   Dept. of Mathematics & Physics
   North South University, Dhaka-1229

   Member
   (External)

II

AUTHOR'S DECLARATION

I hereby declare that the work which is being presented in this thesis entitled "A NUMERICAL INVESTIGATION WITH SENSITIVITY ANALYSIS OF HEAT TRANSFER PERFORMANCE IN A HEAT EXCHANGER CONTAINING NANOFLUIDS" submitted in the partial fulfillment of the requirement of the degree of Master of Philosophy (M.Phil.), Department of Mathematics, Bangladesh University of Engineering and Technology (BUET), Dhaka-1000, Bangladesh, is an authentic work of my own.

The work is also original except attached with special references in the context. No part of this work has been submitted for any attempt to get any other degrees of diploma.

16/04/2023
Saiful Islam
M.Phil. student
Student ID: 0419093002P
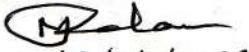Registration No.: 0419093002P
Session: April-2019
Department of Mathematics
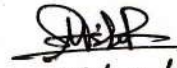Bangladesh University of Engineering and Technology (BUET)
Dhaka-1000, Bangladesh

CERTIFICATE OF RESEARCH

This is certifying that the present work in this thesis entitled "**A NUMERICAL INVESTIGATION WITH SENSITIVITY ANALYSIS OF HEAT TRANSFER PERFORMANCE IN A HEAT EXCHANGER CONTAINING NANOFLUIDS**" has been carried out by the author Saiful Islam, M.Phil. student, Department of Mathematics, Student ID: 0419093002P, Registration No.: 0419093002P, Session: April-2019, under the direct supervision of **Dr. Md. Mustafizur Rahman**, Professor, Department of Mathematics, Bangladesh University of Engineering and Technology (BUET), Dhaka-1000, Bangladesh. The prepared thesis can be accepted in the partial fulfillment of the requirements for the degree of Master of Philosophy (M.Phil.) in Mathematics. The results embodied in this thesis have not been submitted elsewhere for the award of any degree.

16/04/2023

Dr. Md. Mustafizur Rahman
Professor
Department of Mathematics
Bangladesh University of Engineering
and Technology (BUET)
Dhaka-1000, Bangladesh

16/04/2023

Saiful Islam
Student ID: 0419093002P
Registration No.: 0419093002P
Session: April-2019
Department of Mathematics
BUET, Dhaka-1000, Bangladesh

Dedicated

to

My Respectable Parents

ACKNOWLEDGEMENTS

ABSTRACT

The innovative uses of nanofluids in thermal engineering, biomedical engineering, and manufacturing processes have made this field of research interesting on a global scale. In view of such significant applications, the goal of this work is to look into the thermal performance of nanofluid inside a hexagonal heat exchanger. This examines mixed convective phenomena for fluid flow with heat transfer of Titanium Oxide (TiO_2) and water (H_2O) based nanofluid. A hot cylinder on the left portion and another cold cylinder on the right portion are taken horizontally to form a heat exchanger. All of the surrounding walls are considered adiabatic where a magnetic field is acted on the right walls. The Galerkin weighted residual technique of finite element method is utilized to execute the governing equations numerically. The investigation is carried out for the Reynolds number ($Re = 10$-200), Richardson number ($Ri = 0.01$-10), Hartmann number ($Ha = 0$-100), and nanoparticle volume fraction ($\phi = 0$-0.1), which are some relevant parameters. Streamlines, isotherm lines, velocity fields, and average Nusselt numbers (Nu_{av}) are used to depict the collected results. The response surface methodology is used to conduct a sensitivity analysis of independent variables on response function. It is observed that growing value of Re and ϕ strengthen the thermal performance of nanofluid whereas increasing Ha causes it to decrease. When Ha is maintained at 0, the Nu_{av} reaches its maximum values at $Re = 200$ and $\phi = 0.1$. Moreover, ϕ and Re have positive sensitivity to the Nu_{av} while Ha has negative sensitivity. The results of this study may assist engineers and researchers for creating effective mixed convective heat exchangers.

CONTENTS

Nomenclature:

B_0 :   Magnetic field strength (N.A^{-1}.m^{-2})

c_p :   Specific heat (J.kg^{-1} .K^{-1})

g :   Acceleration for gravity (m.s^{-2})

H :   Enclosure height (m)

Ha :   Hartmann number

k :   Thermal conductivity (W.m^{-1} .K^{-1})

L :   Enclosure length (m)

p :   Dimensional Pressure (N.m^{-2})

P :   Dimensionless pressure

Pr :   Prandtl number

Re :   Reynolds number

Nu :   Nusselt number

S :   Surface (m)

t :   Dimensional time (s)

T :   Dimensional temperature (K)

u_0 :   Lid velocity (m.s^{-1})

u, v :   Dimensional velocity component (m.s^{-1})

U, V :   Dimensionless velocity component

x, y :   Dimensional Cartesian coordinates

X, Y :   Dimensionless Cartesian coordinates

TiO_2 :   Titanium Oxide

H_2O :   Water

Greek symbols:

α :   Thermal diffusivity (m^2 .s^{-2})

β :   Coefficient of thermal expansion (K^{-1})

ϕ :   Particle concentration

θ :   Non-dimensional temperature

v :   Kinematic viscosity (m^2 .s^{-1})

μ :   Dynamic viscosity (kg.m^{-1} .s^{-1})

ρ :   Density (kg.m^{-3})

Ω :   Vorticity vector

ψ :   Stream function

σ :   Electric conductivity ($\Omega^{-1}.\ m^{-1}$)

Subscripts:

av	:	Average
bf	:	Base fluid
nf	:	Nanofluid
c	:	Cold surface
h	:	Heat surface
sp	:	Solid particle

Abbreviations:

2D	:	Two dimensional
3D	:	Three dimensional
CCD	:	Central Composite Design
LBM	:	Lattice Boltzmann method
EFDM	:	Explicit finite difference method
FC	:	Face-centered
FDM	:	Finite difference method
EFDM	:	Explicit finite difference method
IFDM	:	Implicit finite difference method
FEM	:	Finite element method
FVM	:	Finite volume method
TDMA	:	Tri-diagonal matrix algorithm
MHD	:	Magnetohydrodynamics
RSM	:	Response surface methodology
Nu_{source}	:	Heat transfer rate from hot left cylinder
Nu_{sink}	:	Heat acceptance rate by cold right cylinder
Nu_{loc}	:	Local Nusselt number

LIST OF FIGURES

LIST OF TABLES

CHAPTER 1
Introduction and Literature Review

1.1 Introduction

Nowadays, an important research topics known as Computational Fluid Dynamics (CFD) is utilized to address numerous industrial and engineering problems in the fields of mechanical engineering, chemical engineering, biomedical engineering, aeronautical engineering and civil engineering. Actually, CFD deals with numerous computational techniques on Fluid Dynamics which relates to fluid flow and heat transfer of liquids and gases. Moreover, the hydrodynamics and the aerodynamics are two branches of fluid dynamics. The analysis of heat transfers and fluid flow behavior on distinct enclosure and over surfaces has already received a vast attention today's researchers due to the existence of fluid about every sector of human life and uses. Not only in terms of thermal energy but also in terms of forecasting the rate of heat exchanges that take place under specific circumstances. Heat is transported due to the variance in temperature switching between systems in the field of heat transformation science.

1.2 Fluid

A substance with surface tension and the ability to flow is called a fluid. In other words, a fluid is something that continuously deforms under shear force. Two sorts of fluids are available: liquids and gases. For all intents and purposes, liquids are considered incompressible fluids while gases are considered compressible fluids. Five physical characteristics of real fluids include density, volume, temperature, pressure and velocity.

1.3 Classification of Fluid

1.3.1 Compressible and Incompressible Fluid

The variation of a fluid's density with relation to changes in pressure is referred to as compressibility. If a fluid's pressure variation matches its density variation, such as air, the fluid is said to be compressible. That is,

$$\frac{\partial \rho}{\partial p} \neq 0 \tag{1.1}$$

where ρ and p are the density and pressure of fluids respectively. If a force applied to a fluid does not alter its density, the fluid is said to be incompressible such as water, engine oil, human blood, etc. That is, for incompressible fluid:

$$\frac{\partial \rho}{\partial p} = 0 \tag{1.2}$$

1.3.2 Ideal and Real Fluid

Ideal fluid is assumed to has zero viscosity $(\mu = 0)$ and incompressible; hence there is no tangential force between adjacent fluid layers. In other words, a perfect fluid has no internal resistance to changing its shape. Whether the fluid is at rest or in motion, the pressure at each point of an ideal fluid is the same in all directions. It is an imagined fluid because in nature none of the other fluids have these characteristics. However, only a few liquids, such as water, which has a constant viscosity, may be regarded as ideal for all practical uses.

On the other hand, when a layer of fluid flows past an adjacent layer in real fluids, both tangential and normal strains are present. In a real fluid, these tangential and frictional forces are linked to a characteristic known as viscosity. Internal friction, which is what causes it, is a significant factor in fluid motion. During the motion, it provides resistance to shearing stress. In contrast to solids, this resistance is dependent on the rate of deformation rather than the deformation itself. Actually, every liquid found in nature is a real fluid. Newtonian fluid and non-Newtonian fluid are the two subcategories of real fluids.

1.3.3 Newtonian and non-Newtonian Fluid

Generally, the term "Newtonian fluid" refers to a fluid that complies with Newton's law of viscosity, whereas the Newtonian's law of viscosity is mathematically defined as:

$$\tau = \mu \frac{du}{dy} \tag{1.3}$$

where τ, μ, and du/dy denote the share stress, dynamic viscosity, and rate of share deformation of a fluid respectively. Examples of Newtonian fluids that can withstand the spectrum of shear loads and shear rates found in daily life include water, air, alcohol, glycerol, and thin motor oil. Conversely, the term "non-Newtonian fluid" refers to a fluid that don't comply with Newton's law of viscosity is called non-Newtonian fluid. Such fluid exhibits nonlinear relationships between shear stress and shear rate.

For example, human blood, Casson fluid, Maxwell fluid, Carreau fluid, etc. Due to their variety, non-Newtonian fluids are categorized by introducing various constitutive models.

1.3.4   Viscous and Inviscid Fluid

If a fluid is subject to both shearing and normal forces, it is said to be viscous. Honey, Toothpaste, human blood, molasses and heavy oil treated as viscous fluid. When a fluid does not exert any shearing force either at rest or in motion, it is said to be non-viscous or inviscid. It is obvious that the pressure that an inviscid fluid applies to any surface is always along the surface's normal at the point. Every gas is regarded as an inviscid fluid.

1.4 Different Types of Fluid Flow

1.4.1   Laminar and Turbulent Flow

Laminar flow is defined as a flow in which each fluid particle carves out a distinct curve and where no two individual fluid particles' curves cross. Conversely, a flow is described as turbulent when each fluid particle does not trace out a distinct curve and when the curves that the fluid particles do trace out intersect.

1.4.2   Steady and Unsteady Flow

Pressure, velocity, temperature, density and other fluid parameters can all be considered functions of time or space. It is referred to as steady flow if the liquid flow properties at every location in the flow field are independent of time. Mathematically, steady flow is defined as:

$$\frac{\partial P}{\partial t} = 0 \qquad (1.4)$$

where P stands for the properties of fluid, which could be pressure, velocity, temperature, density, etc. On the other hand, unsteady flow, also known as non-steady flow, is a flow in which the fluid's flow parameters (such as pressure, velocity, temperature, density, and other variables) change with time. Any process often starts with an unstable fluid flow that could eventually become steady or zero flow. As an illustration, the water flow in a newly opened tap initially fluctuates before becoming stable after a few repetitions. In mathematics, unsteady flow is represented as:

$$\frac{\partial P}{\partial t} \neq 0 \qquad (1.5)$$

1.4.3   Uniform and Non-uniform Flow

When a flow's conditions and attributes are independent of the direction the fluid is traveling in or when all of the fluid's particles have the same magnitude and direction of velocity vector at any given time, the motion is said to be uniform. For instance, a liquid flowing uniformly via a long straight pipe is an example of uniform flow.

On the other hand, non-uniform flow is defined as a flow in which all fluid particles move at the same speed across each segment of a pipe or channel, causing the flow characteristics at any one time to vary with distance. For instance, the flow of a liquid via a curved conduit is not uniform.

1.4.4   Rotational and Irrotational Flow

Rotational flow is characterized by the fluid particles continuing to revolve about their own axes while trailing. On the other hand, a flow is considered irrotational if the fluid particles follow but do not spin about their own axes.

1.5   Modes of Heat Transfer

The manner of thermal energy moving from one area to another due to a temperature differential is known as heat transfer. Conduction, convection, and radiation are the three major techniques or modalities by which heat is transferred. A higher temperature medium is always used to transfer heat to a lower temperature medium, and the process ends when the two mediums achieve the identical temperature.

1.5.1   Conduction

Conduction is the process by which energy is transferred from a substance's higher-energy particle to nearby less-energetic ones due to the contacts between the particles. In solids, liquids, or gases, conduction can occur. Conduction occurs when molecules collide and diffuse as they move randomly through gases, liquids, and solids. In solids, conduction occurs when molecules vibrate in a lattice and free electrons convey energy. The geometry, thickness and material of a medium, as well as the temperature variance through the medium, all affect the rate of heat conduction through it. We may see numerous examples of conduction all around us.

Due to energy conduction through the spoon, the exposed end of a metal spoon that is unexpectedly submerged in a cup of boiling tea will ultimately become warmed. A heated room loses a lot of energy throughout the winter to the outside air. Since it conducts heat, the composite wall separating the interior environment from the exterior is mostly to blame for this loss.

1.5.2 Convection

In the existence of bulk fluid motion brought on by the temperature variance, convection is the mechanism through which heat is transferred through a fluid. Convection is the name for this form of heat transmission. Natural convection and forced convection are the two types of convection used in heat transfer. Natural (or free) convection is the term used when the fluid flow caused by convection happens naturally. In most cases, natural convection has happened as a result of the temperature differences within an enclosure and the buoyancy forces. In this instance, buoyancy effects coming from the density variance induced by the fluid's temperature difference and gravitational force set up fluid motion. On the other hand, forced convection is the heat transmission mode where the fluid motion is artificially produced by an external pressure, inlet velocity, lid velocity, etc. When forced convection occurs, an external factor such as a lid velocity, external pressure and rotational velocity is used to compel the fluid to flow over a surface or inside a pipe. Convection is used to move heat through a fluid when there is bulk fluid motion, whereas conduction is used when there is no fluid motion. Therefore, it is possible to think of conduction as the limiting case of convection in a fluid that leads to the situation of quiescent fluid due to the absence of fluid motion at solid surfaces. Moreover, the combination of natural convection and force convection is known to mixed convection that has numerous industrial and engineering applications. That is, for a mixed convective heat transfer process, there will have an external factor to force, and the buoyancy force will act due to temperature differences on entire fluid domain.

1.5.3 Radiation

Radiation is the name for the energy that matter emits as electromagnetic waves (or photons) in response to changes in the electrical structure of the atom or molecule. Heat can be transferred by radiation without the need for an intermediary medium, in contrast to conduction and convection.

Actually, in a vacuum, radiation-based heat transfer is more rapid and exhibits no attenuation. The sun's energy enters the planet in this way. All solids, liquids, and gases emit, absorb, or transmit radiation to variable degrees since it is a volumetric phenomenon. When it comes to solids like metals, wood, and rocks, which are opaque to heat radiation, radiation is typically thought of as a surface phenomenon.

1.6 Base Fluid

The conventional available fluid serves as the base fluid in thermal engineering. The use of numerous dissimilar liquids with low thermal conductivity as base fluid is successful and efficient. These liquids include water (H_2O), engine oil, ethylene glycol, pump oil, bio-fluids, kerosene, glycerol and other lubricants, and so on. Many of them work in a variety of industrial settings and engineering fields.

1.7 Nanofluids

Nanofluids are fluid suspensions of nanoparticles that exhibit a considerable improvement in their characteristics at low nanoparticle concentrations. As engineering equipment get smaller, there is a growing need to speed up heat transmission in tiny devices like micro-sensors and laser crystals. Adding nanoparticles to the base fluid, often known as nanofluid, is one way to solve this issue. A novel type of heat transmission fluid named a nanofluid is made up of a small number of uniformly distributed, stable nanoparticles (such as: Cu, CuO, TiO_2, Al_2O_3, etc.,) with a diameter of less than 100 nm. In Figure 1.1, a sample of Titanium oxide (TiO_2) nanoparticles is represented. Argonne National Laboratory came up with the term "nanofluids" to designate a fluid in which nanometer-sized particles are suspended.
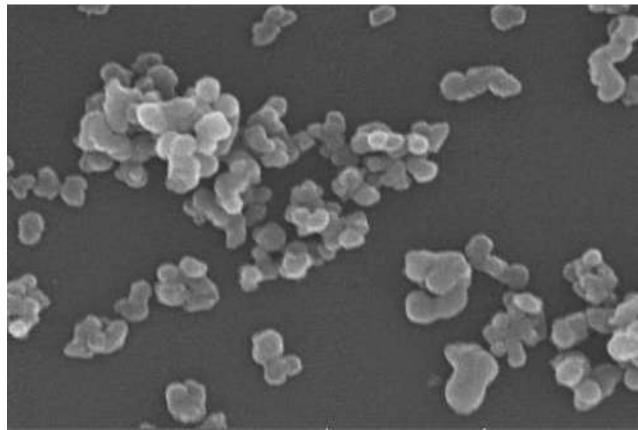
Figure 1.1: Titanium oxide nanoparticles [1].

The thermal conductivity and convective heat transfer capabilities of the base liquids have been proven to be improved by nanofluids made up of such particles suspended in liquids (usually conventional heat transfer liquids). Even at low volume concentrations, nanofluids significantly improve thermal performance since their thermal conductivities are often orders-of-magnitude better than those of the base fluids like water, ethylene glycol, and light oils. In Figure 1.2, the process of nanofluid formation is shown by using nanoparticles and base fluid. In comparison to basic fluids like oil or water, the thermal conductivity, thermal diffusivity, viscosity and convective heat transfer coefficients of nanofluids have all been found to be improved over those of conventional fluids.

It is obvious from the current review that nanofluids have improved thermal conductivity, and that this conductivity increases as the volumetric percentage of nanoparticles increases. Nanofluids have thermal properties that are considerably different from those of traditional heat transfer fluids, according to study findings from nanofluid research groups throughout the world. The thermal conductivity augmentation of various nanoparticles in a variability of fluids with volume concentrations in the range of 0.5-4% has been determined by several researchers, as will be addressed further. Because these can be employed in a wide range of industrial and engineering applications, including heat exchangers, biomedical engineering, chemical production, computer processors, transformer cooling, and others, nanofluids are significant. Therefore, it is crucial to undertake additional study in order to determine how these parameters affect the thermal conductivity of a variety of nanofluids.
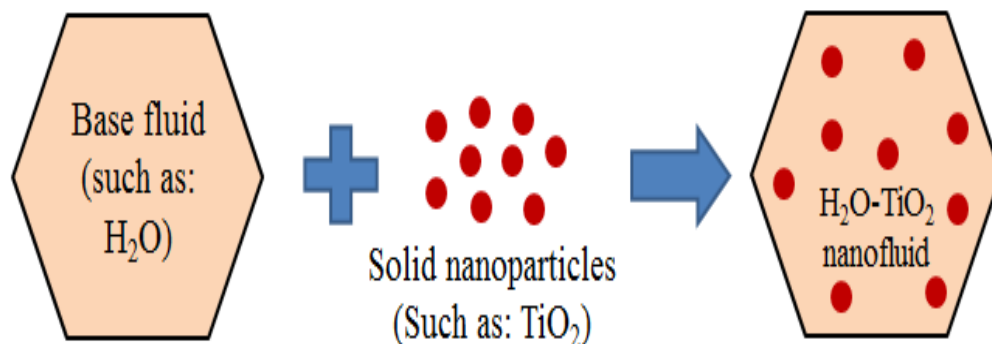
Figure 1.2: Formation of nanofluid.

1.8 Solid Volume Fraction of Nanoparticles

The volumetric fraction, size, and shape of the nanoparticles have an impact on the properties of the nanofluid. The volume of all the nanofluid ingredients is divided by the nanoparticle volume fraction (ϕ). When the volumes of the constituents are additive, the volume fraction and volume concentration coincides in an ideal solution. In other words, the solution's volume is the same as the total volume of the nanoparticles. The volume fractions of the solution added together equal to one.

That is,

$$\sum_{i=1}^{M} \phi_i = 1 \tag{1.6}$$

where M is the total number of nanoparticles in a nanofluid.

1.9 Magnetohydrodynamics

The study of magnetohydrodynamics (MHD) explains how magnetic fields affect electrically conducting liquids. The terms magneto, hydro, and dynamics, which collectively denote a magnetic field, a liquid or fluid, and movement, respectively, are the basis for the theory of MHD. The movement of liquid or gaseous electrically conducting fluids in electric and magnetic fields is the subject of this subfield of magneto fluid dynamics. MHD is heavily invested in the fields of cooling of fission and fusion reactors, nuclear fusion, earth magnetic field, X-ray radiation, electrolytes, star formation, plasmas, tumor therapy, solar wind, etc. Several researchers looked at MHD heat transport in various cavities as a result of these practical applications at various times. In order to link the flow field and dynamics equations, it examines the dynamics of a substance moving in an electromagnetic field where currents are created in the material by induction modified field. By moving the conducting fluid, which affects the magnetic field as well as the action of the magnetic field, electrical currents are produced with the help of the magnetic field's influence. The magnetic field's impact helps to increase the mechanical forces, which change how fluid flows. Electromagnetic forces will be produced for the weak electrical conductivity, whether it is gases or liquids, and these might have a similar strength to the hydrodynamic and inertial forces.

1.10 Viscosity

Real fluids have a characteristic called viscosity that makes them resistant to shearing and allows particles to slide through or close to one another. Viscosity is often referred to as fluid internal friction. This characteristic exists in various degrees in all known fluids. Fluids with low viscosity include water, alcohol, and air; whereas, fluids with high viscosity include oils, glycerin, and other substances. Generally, viscosity is denoted by μ.

1.11 Kinematic Viscosity

The ratio of absolute viscosity to density is known as the kinematic viscosity. It is denoted by ν, and it is defined as:

$$\nu = \frac{Vis\cos ity}{Density} = \frac{\mu}{\rho} \tag{1.7}$$

It is noted that, for water, gases, and alcohol μ is very small but not insignificant values, but for oil and glycerin μ is quite big values. Also, for a large number of fluids, μ relies on both pressure and temperature, whereas μ is inversely proportional to temperature and independent of pressure for gases.

1.12 Useful Dimensionless Parameters

1.12.1 Prandtl Number

The Prandtl number (*Pr*), a non-dimensional quantity, essentially corresponds to the relationship between momentum diffusivity (kinematic viscosity) and thermal diffusivity. It bears the name Ludwig Prandtl in honor of the German physicist who developed the idea of the boundary layer in 1904 and made substantial contributions to the theory of the boundary layer. Heat diffuses very slowly in liquids relative to momentum, which is represented by a large Prandtl number (*Pr* >> 1) in the behavior. In contrast, a low Prandtl number (*Pr* << *1*) denotes the dominant thermal diffusivity, which means that heat moves through liquids relatively quickly. *Pr* = 1 (about) means that both heat and momentum diffuse through the fluid at roughly the same rates. Mathematically, Prandtl number is defined as:

$$\text{Pr} = \frac{Momentum\ diffusivity}{Thermal\ diffusivity} = \frac{\nu}{\alpha} = \frac{\mu/\rho}{k/\rho c_p} \tag{1.8}$$

where $\nu, \alpha, \mu, k, \rho$, and c_p indicate the kinematic viscosity, thermal diffusivity, dynamic

viscosity, thermal conductivity, density of fluid, and specific heat at constant pressure respectively.

1.12.2 Reynolds Number

Laminar flow changes to turbulent flow depending on a number of factors, including fluid type, flow velocity, surface temperature, and surface geometry. To clarify the change from laminar to turbulent flow Osborn Reynolds made the important discovery in 1883 that the ratio of the fluid's inertia forces to viscous forces regulates the flow organization.

In fact, the Reynolds number (*Re*) that is a dimensionless number aids in the prediction of fluid flow patterns in many circumstances. Laminar flow typically predominates in flows with low Reynolds numbers, while turbulent flow typically predominates in flows with high Reynolds numbers. The Reynolds number that encapsulates this ratio is written as:

$$\text{Re} = \frac{Inertia\ force}{Viscous\ force} = \frac{uL}{v} = \frac{\rho uL}{\mu} \tag{1.9}$$

where u, L, μ, and ρ represent the magnitude of fluid flow velocity, characteristic length of fluid domain, dynamic viscosity, and density of fluid. Also, $v = \frac{\mu}{\rho}$ is known as kinematic viscosity of fluid.

1.12.3 Grashof Number

Grashof, a German scientist, number (*Gr*) is a dimensionless number which measures the proportion of the buoyancy force to the fluid's viscous forces, and determines the flow regime in free convection. Mathematically, it is defined as:

$$Gr = \frac{Bouyancy\ force}{Viscous\ force} = \frac{g\beta L^3 \left(T_w - T_\infty\right)}{v^2} \tag{1.10}$$

where $g, \beta, L, T_w, T_\infty$, and v represent the acceleration due to gravitational force, thermal expansion coefficient, characteristic length of fluid domain, wall temperature, ambient temperature, and kinematic viscosity respectively. The Reynolds number's function plays significant role in forced convection, whereas the Grashof number's function plays in free convection. In order to determine whether the fluid is laminar or turbulent during free convection, the Grashof number serves as the primary criterion. Moreover, *Gr >0* and *Gr <0* are used for cooling and heating Newtonian fluids respectively.

1.12.4 Richardson number

The English mathematician Lewis Fry Richardson is honored by having his number, the Richardson number (*Ri*), named after him. It is a dimensionless number that represents the proportion of the buoyancy term to the flow shear term. It illustrates the significance of natural convection in thermal convection problems as comparison to forced convection. Mathematically, Richardson number is defined as:

$$Ri = \frac{Gr}{\mathrm{Re}^2} \tag{1.11}$$

where *Gr* and *Re* denote the Grashof number and the Reynolds number respectively.

1.12.5 Hartmann number

A non-dimensional quantity called the Hartmann number (*Ha*), firstly introduced by Julius Hartmann, represents the proportion of electromagnetic force to viscous force. This non-dimensional number gauges the significance of drag forces brought on by magnetic effects and viscous forces. It describes conducting fluid flow in a transverse magnetic field as well. Due to the fact that it is a function of the magnetic flux density, characteristic length, and the square root of the electrical conductivity to viscosity ratio. Mathematically, the Hartmann number defined as:

$$Ha = \frac{Electromagnetic\ force}{Viscous\ force} = B_0 L \sqrt{\sigma/\mu} \tag{1.12}$$

where $\beta_0, L, \sigma,$ and ν express the magnetic field, characteristic length, electrical conductivity, and kinematic viscosity of fluid respectively.

1.12.6 Nusselt Number

The Nusselt number (*Nu*) is a non-dimensional number that shows how convection, as opposed to conduction, increases the amount of temperature that may be transported throughout the fluid layer. It is named after a German scientist Wilhelm Nusselt at the beginning of the twenty-first century. It shows how much more heat is transported when a fluid is moving as opposed to when heat is transferred through conduction. *Nu* significantly influenced convection temperature transport. The larger value of *Nu* denotes strong temperature convection transport and a big temperature gradient at the surface.

According to the $Nu = 1$, fluid is immobile and all temperature is transferred through conduction. Mathematically, Nusselt number defined as:

$$Nu = \frac{Convective\ heat\ transfer}{Conductive\ hea\ transfer} = \frac{hL}{k} \tag{1.13}$$

where h, L, and k indicate the heat transfer coefficient, characteristics length of fluid domain, and thermal conductivity of the fluid respectively.

1.13 Background of the Study

A current focus of scientific and engineering research is on nanofluid flow due to its rapid heat exchanging rate. The enrichment of heat transfer rates in industrial processes such as heat exchangers, microelectronics, cooling of electronic tools, solar water heating, solar collector, fusion reactors, computer processors, nuclear reactor cooling, transformer cooling and mineral oils is made possible by this significant scientific phenomenon [2-6]. Since nanofluid offer innovative prospects to improve heat transfer enactment with respect to pure liquids, it can be predicted to become the subsequent-generation heat transfer fluids. Correspondingly, there are distinct biomedical uses for nanofluids, including the treatment of cancer and the delivery of drugs. A suitable suspension of common liquids (base fluid) and nanometer size solid particles (Cu, CuO, TiO_2, Fe, Al_2O_3, etc.,) is called a nanofluid. First of all, in 1995, Choi [7] introduced nanofluid at Argonne National Laboratory in the USA. This study showed that a conventional fluid's thermal characteristics can be boosted by the addition of nanoparticles into base fluid (water, motor oil, pump oil, etc.). Sheikholeslami et al. [8] employed the Lattice Boltzmann method (LBM) to talk over the physical appearance of heat transfer of Al_2O_3-H_2O nanofluid flow in a semi-annular enclosure including the consequences of magnetic field. It was discovered that the average Nusselt number (Nu_{av}) was a decreasing function of Hartmann number, whereas the average Nusselt number was an accumulative function of the Rayleigh number and the nanoparticle volume fraction. In a triangular cavity, Rahman et al. [9] analyzed the performance of heat transfer for Cu-H_2O nanofluid in a mixed convective inclined lid-driven triangular cavity, where the Nu_{av} on the hot surface was used to describe the overall heat transfer rate of the heated surface. On the flow and heat fields, it was explored that the tilt angle and the solid volume fractions had a considerable impact.

Additionally, the solid volume percentage was optimized to produce the maximum heat transfer rate for the evaluated Richardson numbers (*Ri*). Cimpean et al. [10] examined mixed convection in a porous trapezoidal chamber filled with a hybrid nanofluid to accelerate the rate of heat transfer. By selecting various suitable nanoparticle amalgamations in hybrid nanofluid, the anticipated heat transfer rate may be accomplished, according to calculations made using the change of the fluid flow and heat transfer rate. Another investigation on mixed convective hybrid nanofluid was described by Ghadikolaei et al. [11] including the effect of Hydrogen bond. For numerical simulation, Runge- Kutta Fehlberg 5th order (RKF-5) numerical method was used. They came to the conclusion that the Lorentz force brought about by increasing the magnetic square parameter results in a decrease in the velocity profile. Patil et al. [12] investigated hybrid nanofluid on a moving cylinder, where implicit finite difference method was applied to complete the numerical simulation. They found that when hybrid nanoparticles were added to base fluid, heat transmission was increased compared to base fluid and nanofluid. Another investigation about heat and mass transfer appearances using nanofluid on a Riga plate was completed by Vaidya et al. [13]. They used the optimal homotopy analysis (OHA) and concluded that the modified Hartmann number decreased the fluid temperature profile. Likewise, the radiation parameter used to the dissolution of fluid molecule hydrogen bonds. Additionally, recently multiple studies on nanofluid flow were done in order to explore the heat transfer mechanisms in a number of systems [14-18].

Moreover, the present researchers are also interested by mixed convective fluid flow and heat transfer on close cavity, where the amalgamation of natural and force convection is acknowledged as mixed convection. Due to a wide range of applications, including electronics cooling system, heat exchangers, solar panel storage, etc., it has recently attracted a lot of attention in the fields of engineering [19]. In reality, natural convection has taken place automatically because of the temperature difference and buoyant forces in an enclosure whereas the force convection occurs due to external force or pressure into the cavity. That is, for mixed convective analysis these two types of convection are occurred. The cavity's geometry and orientation have an impact on the mixed convection phenomenon. Generally, mixed convection is occurred in a cavity for either lid velocity of any sides of the cavity or created ventilation on cavity. So, a number of investigations on mixed convective heat transfer containing nanofluid have been completed by various researchers.

Using a modified power-law viscosity model, Molla et al. [20] conducted a computational investigation on mixed convective heat transport of non-Newtonian fluids on a flat plate. Beg et al. [21] explored mixed convective nanomaterial flow through porous space originating from exponential stretched sheet. Explicit finite difference method (EFDM) was utilized to complete that simulation where stability and convergence test were performed. It was discovered that the flow accelerated with rising thermal and species Grashof numbers, rising Brownian motion, and rising thermophoresis effects. Hatami et al. [22] analyzed the mixed convective phenomenon by taking lid velocity in a T-shaped porous cavity that contain nanofluids, where the impact of various nanoparticles (Cu, TiO_2, Al_2O_3) and their volume fraction was studied. For optimization purpose the response surface methodology (RSM) was used in that work. Additionally, the impact of various nanoparticles and their volume fraction on the Nusselt number was examined. Another investigation on mixed convection with magnetic field was performed by Alshare et al. [23]. The cavity's lower part had wavy boundary heated condition that was filled with nanofluid. In their analysis, they found that the entropy formation was mostly caused by heat transmission, with only minor contributions from frictional and magnetic phenomena. For a square-shaped cavity, Manchanda et al. [24] examined mixed convection for a non-Newtonian fluid. The top and bottom walls of the square hollow were thermally insulated and kept moving in opposing directions along the X-axis whereas the left and right standing walls are visible to ambient state. In a lid driven cavity, Gangawane et al. [25] described the effects of a block which had a uniform heat flux into this cavity. According to the study's findings, the centered block position transfers heat more quickly than the other two positions. Moreover, in a trapezoidal cavity double-diffusive mixed convective analysis was performed by Mondal et al. [26] with Al_2O_3-H_2O fluid. It was assumed that the cavity's top wall shifted with constant velocity u_0 in the direction of the positive X-axis. By utilizing the biconjugate gradient stabilized approach, the governing equations were solved via second and fourth order finite difference approximations. The main objective was to limit entropy formation caused by the interaction of magnetic field, heat transfer, mass transfer, and fluid flow in order to reduce energy loss.

Furthermore, magnetohydrodynamics (MHD) is the field of research that described the impact of magnetic fields on electrically conducting liquids. The earth's magnetic field, X-ray radiation, nuclear fusion, fission reactor's cooling, solar wind, tumor therapy, etc., are all involved with MHD. Due of these real-world uses, a large number of researchers looked at MHD heat transport in various cavities at various points in time [27-29].

Abderrahmane et al. [30] analyzed mixed convection on a porous triangular cavity, filled by hybrid nanofluid, with rotating cylinder. The well-known finite element technique was utilized for involved governing equations, and founded that the heat transfer rate on that cavity was boosted by increasing Darcy number. Alsedais et al. [31] selected an undulating porous enclosure to analyze mixed convection where a solid obstacle was fixed on the cavity. The finite volume technique was applied to make such a conclusion that the average heat transfer rate developed by 42.86% by growing undulation effect. Parveen et al. [32] investigated the temperature-dependent thermal conductivity of a free convective viscous incompressible fluid in the presence of heat absorption along a vertical wavy surface that was uniformly heated. The Keller-box scheme, an implicit finite difference method (IFDM), was used to solve it numerically. It was found that for the higher values of the temperature-dependent thermal conductivity variation parameter, both the fluid flow and the temperature distribution within the boundary layer greatly increased. Sheikholeslami et al. [33] inspected magnetic field and how radiation affected the suspension of Al_2O_3-H_2O nanofluid in an enclosure with uniform heat flux. In order to simulate the thermal conductivity and the viscosity of a nanofluid, the Koo-Kleinstreuer-Li (KKL) correlation was used. The findings indicated that improvements in heat transfer had a direct link with the Hartmann number and the radiation parameter, but that the Rayleigh number had a reverse relationship. Parveen et al. [34] examined the impact of the temperature-dependent variables viscosity and viscous dissipation on the boundary layer flow of an electrically conducting fluid that is viscous and incompressible along a vertical undulating surface in the existence of a transverse magnetic field. The uniform wall temperature, which was greater than the ambient temperature, was kept at the undulating surface.

The impact of magnetic field for an MHD nanofluid flow on a straight up plate was investigated by Chamkha et al. [35] in the presence of a magnetic field, heat generation or absorption, and suction or injection effects. An effective, iterative, tri-diagonal implicit finite-difference technique was used to numerically solve the governing equations. Another laminar MHD fluid flow model was created by Molla et al. [36] for an isothermal sphere immersed in a fluid whose viscosity was proportional to a linear function of temperature. The very effective IFDM, the Keller box scheme, and a straight numerical strategy were used to resolve the governing equations. To visualize heatline contours for energy transportation, Islam et al. [37] discussed an MHD fluid flow model containing Cu-nanoparticles in a prismatic enclosure.

On that cavity's wall, two types of boundary conditions were applied. The Galerkin weighted residual finite element method was utilized, and came to the conclusion that the thermal boundary condition and form of the nanoparticles are significantly influenced by the heat transfer rate. Including outer magnetic field in a horizontal channel containing Cu-H_2O fluid, Ali et al. [38] performed another mixed convective exploration, where the channel was partially heated. The governing equations were resolved using the finite element method based on the Boussinesq approximation. According to the findings, the height and orientation of alternated baffles had an impact on the flow of fluid and the transfer of heat. Moreover, Jakeer et al. [39] studied MHD Cu-Al_2O_3-H_2O nanofluid in a porous lid driven cavity including Cattaneo-Christov heat flux. Dimensionless versions of the governing equations were numerically computed using the SIMPLER algorithm and the finite volume method (FVM). It was concluded that the in comparison to other nanofluids, the hybrid kind offers a higher rate of heat transmission. Ali et al. [40] quantitatively examined another mixed convective nanofluid flow mode that filled a cavity created by the thermal buoyancy force, a moving wall, and a rotating flat plate exposed to an external magnetic field. At the center of the chamber was a flat plate that rotated counterclockwise, and found that maximum heat transfer was produced by the plate's longer length and faster rotation.

1.14 Motivation of the Research

From the aforesaid literature survey, it is clear that the researchers are very interested in the MHD mixed convective heat exchanger because it has applications in numerous engineering disciplines. Though distinct studies were completed in different time on dissimilar closed cavity to investigate the MHD mixed convective fluid flow and heat transfer behavior but specifically a few studies on hexagonal enclosures holding various nanoparticles have also been done in recent years [41-45]. Once more, a very few studies on heat exchangers (a mechanical device is used to handover heat between two or more fluids) were conducted to create the rapid heat transfer system [46-50]. But in this piece, these two phenomena (mixed convection and heat exchanger) are combined into a hexagonal-shaped cavity.

This means that in this work, the mixed convective heat transfer process for a hexagonal heat exchanger with TiO_2-H_2O nanofluid composition is analyzed including the existence of a magnetic field. As far as the author is aware, this issue has not yet been the subject of any research.

Furthermore, a sensitivity analysis on input parameters is done with the response surface methodology (RSM) by using statistical analyzing software. The analysis of variance (ANOVA) test is performed and explained. The finite element method [51-52] is utilized to simulate the governing equations of this heat exchanger model. The influences of involved parameters are discussed graphically and physically. The manner of heat transfer rate is explained in details by average Nusselt number (Nu_{av}). Also, streamlines and isotherm lines are explained with the changes of involved factors. The primary goal of this research is to examine how this mixed convective heat exchanger is affected by the Richardson number (Ri), Hartmann number (Ha), Reynolds number (Re), and nanoparticle volume fraction (ϕ).

1.15   Main Objectives of the Study

The present study examines numerically time-independent mixed convective heat transfer process with sensitivity analysis inside a hexagonal heat exchanger filled in TiO_2-H_2O nanofluid composition with the presence of a magnetic field. The outcomes of various involved parameters such as Reynolds number (Re), Richardson number (Ri), Hartmann number (Ha), and nanoparticles volume fraction (ϕ) will be presented in terms of streamlines, isotherms, and Nu_{av}. The following are the primary goals of the planned study:

a) To develop an appropriate mathematical model for exploring the fluid flow and heat transfer characteristics for a mixed convective hexagonal heat exchanger that contains nanofluids.

b) To solve the governing equations numerically using the Galerkin weighted residual finite element method.

c) To evaluate the thermal efficiency of heat exchangers with or without existence of nanofluids.

d) To analyze the influence of involved parameters, namely Reynolds number (Re), Richardson number (Ri), Hartmann number (Ha), and nanoparticle volume fraction (ϕ) for heat transfer enhancement.

e) To develop a best fitted mathematical correlation among independent factors and response function, and discussed sensitivity analysis by using response surface methodology for these independent factors of this model.

f) To compare the obtained results with published work, and publish this research into a good scientific journal.

1.16 Outlines of the Thesis

The consequences of steady mixed convective fluid flow and heat transfer of a hexagonal heat exchanger that contains TiO_2-H_2O nanofluid under the control of a constant magnetic field are examined in this inquiry. Some important ideas about this subject, the principles of nanofluids and pertinent discussion on dimensionless parameters have been provided in Chapter 1. The literature overview of previous investigations on fluid flow and heat transfer in various cavities or channels is briefly discussed here. Additionally, a succinct introduction is provided along with the primary goals and sources of motivation for choosing the current study. The computational techniques that are usually used to solve governing equations have discussed in Chapter 2. Also, the mathematical modelling of proposed model is also described here. Moreover, a set of transformation variables has used to convert the nonlinear governing partial equations with boundary conditions into a non-dimensional form. Furthermore, the finite element method's formulation and result comparison have discussed in details in Chapter 2. In Chapter 3, the outcomes of involved parameters, such as, Reynolds number (Re), Richardson number (Ri), Hartmann number (Ha) and nanoparticle volume fraction (ϕ) have explained in terms of streamlines, isotherm lines and average Nusselt number (Nu_{av}) from a physical point of views. Also, the sensitivity analysis about involved factors on Nu_{av} has been discussed with the response surface method (RSM). Finally, in Chapter 4, a summary of the major accomplishments and some suggestions for future work have been provided.

CHAPTER 2

Computational Techniques & Mathematical Modelling

2.1 Computational Fluid Dynamics

The study of thermodynamic flow and heat transfer can be done theoretically or experimentally. Due to their restricted flexibility and applications, experimental study of such problems was unable to become very prominent in the field of thermodynamics. Since it takes a long time and costs to solve fluid flow issues experimentally, the computational fluid dynamics (CFD) method is growing in popularity for technological and scientific objectives. Fluid dynamics is not flexible enough to allow for adequate experimental examination of temperature transport and fluid movement. Ordinary or partial differential equations, which have been the focus of analytical and numerical research, may be used to represent numerous complex physical models mathematically. But due to the involvement of complex geometric entities, numerous variables, nonlinearity in governing equations, various boundary forms, and circumstances, the straight-forward analytical methods of solution are not also more beneficial. Therefore, the best choice for solving real-world partial differential equations issues is to use numerical methods. CFD is utilized to tackle such engineering problems via computer-based simulation for sophisticated geometry or some crucial aspect that cannot be solved using a regular method. A practical approximation of a natural living system, CFD uses information from a set of algebraic equations. The results of the computational process can be used to comprehend a system's performance. In order to create realistic physical solutions with appropriate accuracy, researchers use CFD simulation software using finite grids. Complex geometry's precise and reliable prophecy more than meets the intense demand for increased superior reliability and economic challenges. These phenomena typically occur in CFD, which has been used for years to numerically calculate fluid dynamical model. Today, it is successfully used to large-scale industrial and engineering challenges, such as laminar flow, turbulent flows, compressible flow, single phase flow, two phase flow, etc.

2.2 Discretization Methods

In order to approximate the differential equations for the variable at a set of discrete locations in space and time, one must first select a suitable mathematical model. Next, one must select an appropriate discretization scheme. Accordingly, each element of a differential equation is converted into a numerical analog, characterized in a computer, and then deal with a software application based on an algorithm. With regard to the high-performance numerical calculation in CFD, a number of discretization techniques are available, including the finite difference method (FDM), finite volume method (FVM), finite element method (FEM), boundary element method (BEM) and boundary volume method (BVM).

2.2.1 Finite Difference Method

The finite difference method (FDM) is the earliest technique for numerically solving PDEs, and Euler is thought to have developed it in the eighteenth century. The conservation equation in differential form serves as the starting point, and a grid is used to define the solution domain. By substituting approximations in terms of the nodal values of the functions for the partial derivatives at each grid point, the differential equation is roughly approximated. As a result, each grid node has a single algebraic equation, in which the unknowns are the variable value at that node and a specific number of its neighbors. Although it is typically used for structured grids, the FDM can be applied to any form of grid. The grid lines also act as lines of local coordinates. The first and second derivatives of the variables with respect to the coordinates can be approximated using polynomial fitting or the Taylor series expansion. These techniques can also be utilized, if necessary, to get variable values away from grid nodes. It is simple to understand and utilize. Although the FDM has a few benefits, it is extremely challenging and nearly impossible to perform when dealing with complex geometric body shapes and boundary constraints.

2.2.2 Finite Volume Method

The integral form of the conservation equations serves as the foundation for the finite volume method (FVM). The conservation equations are applied to each of the finitely many contiguous control volumes (CVs) that make up the solution domain. A computational node where the variable values are to be determined is located at the centroid of each CVs. To translate variable values at the CV surface into nodal values, interpolation is used. Suitable quadrature equations are used to approximate surface and volume integrals.

The output is an algebraic equation for each CV that contains a number of neighbor nodal values. The grid need not be connected to a coordinate system and just sets the control volume limits. By design, the approach is conservative, provided that the surface integrals-which represent the convective and diffusive fluxes-are the same for the CVs that share the borders. It is favored by engineers since it has physical meaning for all terms that must be approximated. However, this computational strategy has a drawback in comparison to other computational techniques in that it is more challenging to build methods in three dimensions for orders higher than two. This is because interpolation and integration are the two levels of approximation required by the FVM. Additionally, the geometric body shape is intricate, and managing the boundary conditions is quite challenging.

2.2.3 Finite Element Method

Each numerical approach for solving partial differential equations has certain strengths and some weaknesses. When all other techniques have failed, finite element method (FEM) manages complex geometrical bodies and boundaries. The FEM is similar to the FVM in many ways. The domain is divided into a number of discrete, unstructured volumes of finite components; in 2D, these volumes are typically made up of triangles or quadrilaterals, while in 3D, they are most frequently made up of tetrahedral or hexahedra. In FEM, the entire domain (Γ) is partitioned into a number of smaller subdomains known as finite elements (Λ^e). A discretization process for FEM is represented in Figure 2.1 for a 2D domain. An overview about this discretization technique was discussed by Reddy [53]. By using the Delaunay triangular method [54], the current numerical strategy is discretized the computational domain into unstructured triangles. While mesh generation was still in its early stages, the Delaunay triangulation has been a very popular geometric construction.
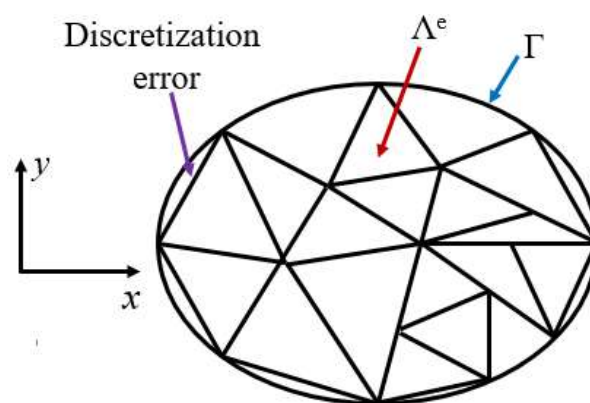
Figure 2.1: Finite element discretization of a two-dimensional domain.

Moreover, the equations that are solved by FEM are multiplied by a weight function before being integrated across the entire domain, which is how FEMs are distinguished from other approaches. The solution is approximated by a linear shape function inside each element in the most basic FEM, ensuring continuity of a solution across element boundaries. From its values in the corners of the elements, such a function can be created. Typically, the weight function takes the same shape. Following that, the approximation is substituted into the weighted integral of the conservation law, and the equations to be solved are derived by requiring that the integral's derivative with respect to each nodal value be zero. This corresponds to choosing the best option from the list of permitted functions. Several non-linear algebraic equations are the end result. The ability to work with any geometry is one of the main benefits of FEM. The grids can be readily improved; just divide each piece. Finite element techniques can be proved to exhibit optimality properties for specific kinds of equations, and mathematical analysis of these techniques is not too difficult. The ability of a particular model to derive the equations for each element before assembly is another benefit of FEM. Mathematical problems involving FEM can be analyzed rather easily.

The finite element technique with Galerkin weighted residuals has been applied in recent numerical computation. It is a highly effective method for computing numerically and approximating solutions to a system of PDEs. The use of FEM in solving fluid dynamics problems has gained prominence over time. For dealing with time-dependent, independent and nonlinear flow issues in irregular domains, this method is sufficiently universal. The mathematical model generation is created by clipping together the local approximations of the phenomena under study, which is a key feature of FEM. The capacity to handle any complicated geometries is the key benefit of FEM. Additionally, the grid may be readily redefined, and each element can be divided easily. FEM generates equations for every component separately from every other component. The interactions between the components are only taken into consideration when the equations are compiled and combined into a global matrix. The majority of the computational techniques for these ideal qualities are dominated by FEM. When the sides of the elements are appropriately aligned and share the same nodes as their adjacent elements, there are no constraints on how the components can be connected in FEM. We are able to represent quite complex geometries because to this flexibility. In fact, a set of discrete volumes of finite elements, which are typically unstructured, are used to divide the domain in FEM. Finite elements in 2D geometry are often made up of triangles or quadrilaterals.

The equations are multiplied by a weight function prior to being integrated over the full domain, which is what makes the weighted residual finite element method unique. In order to ensure continuity of a solution across element boundaries, a linear shape function approximates the solution within each element. Generally speaking, the weight function is a shape function. The weighted integral of the conservation equations is then changed to reflect the approximation. For viscous incompressible thermal flows, in 1999, Dechaumphai et al. [55] applied finite element method. Also, in different time in numerous simulations the FEM is used successfully to simulate distinct complex shape model [5, 9, 30, 38].

2.3 Mathematical Modelling

The first step in any numerical technique is to create a mathematical model of the physical issue at hand, which typically consists of a collection of ordinary and partial differential equations that are either linear or nonlinear and include the necessary boundary conditions. The conservation of mass, momentum, and energy is the foundation of the generalized governing ordinary or partial differential equations. Researchers and scientists are primarily concerned with improving the rate of heat transfer in all thermal systems and industries. Actually, the mixed convective fluid flow and heat transfer analysis is so much essential in industrial and engineering applications such as in heat exchanger, air-conditioning systems, refrigerator, cooling electronic devices, solar collectors, building insulation, etc. As a result, enhancing heat transfer efficacy in these systems is crucial from the standpoint of energy conservation. Improved fluid properties known as nanofluids have many advantages over base fluids that are typically employed in engineering and industrial applications including microelectronics, computer processors, heat exchangers, electrical devices, etc.

Several mixed convective studies completed on numerous cavities containing nanofluid, for example, triangular shape, square shape, prismatic shape, circular shape, hexagonal shape, that have been described in literature review section for different nanofluids. Again, a very few studies on heat exchangers were conducted to create the rapid heat transfer system. So, to the best of my knowledge, no research has yet been done on the literature review pertaining to a mixed convective heat exchanger in the shape of a hexagon that is filled with various nanofluids and is affected by a magnetic field. That is, in this numerical investigation, a study of MHD mixed convective fluid flow and heat transfer for hexagonal shape heat exchanger filled with nanofluid under the influence of the uniform magnetic field has been performed.

Due to its ability to solve complicated problems, the FEM is one of the numerical methods that have gained prominence. The discretization of the governing equations in this study will be accomplished using FEM. The Galerkin finite element method will yield the solution of the governing equations as well as the boundary conditions. The current numerical simulations offer a forecast that may be used for design optimization and the enhancement of thermal performance of energy systems such heat exchangers, solar thermal collectors, biomedical engineering, cooling of electronic appliances, and so on.

2.3.1 Physical Modelling

In this numerical analysis, a mixed convective hexagonal heat exchanger is chosen as a fluid area containing with Titanium oxide (TiO_2) nanoparticles with water (H_2O), which is considered steady, Newtonian, and incompressible laminar fluid including the influence of a magnetic field. This hexagonal enclosure is heat and mass insulated that's height and length is H and L respectively. The top horizontal wall is moving by a lid velocity u_0. Two cylindrical pipes (radius is $0.1L$) are used as a cooler and heater, respectively, on the right and left sides. The configuration of this hexagonal heat exchanger-based fluid model is shown in Figure 2.2. The right cylindrical pipe is considered as a cooled surface T_c, and the left pipe is considered as a hot surface T_h. The fluid domain's exterior walls are completely preserved and insulated. Along the negative direction of the Y-axis, the gravitational acceleration g is acted to this fluid field. Moreover, the enclosure is encased in a constant magnetic field B_0 that extends from the right to the left. The size and form of the TiO_2 nanoparticles are thought to be identical, and adjacent mediums are regarded as non-slip. The nanofluid's thermophysical characteristics are listed in Table 1.
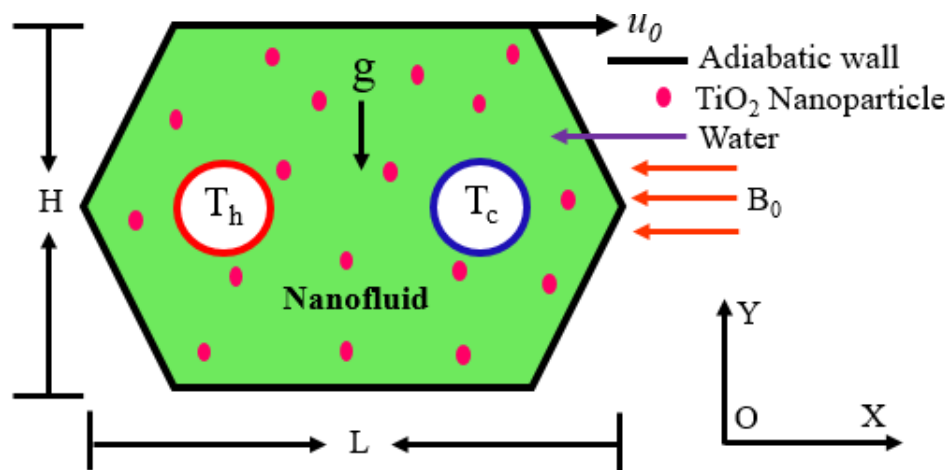
Figure 2.2: Physical configuration of proposed hexagonal heat exchanger.

A two-dimensional (2D) coordinate system is used to view and complete the fluid domain model, with the *X*-axis denoting the bottom wall and the *Y*-axis pointing in the direction of the left sidewall. A 2D coordinate system is used to view the fluid domain model, with the *X*-axis denoting the bottom wall and the *Y*-axis pointing in the direction of the left sidewall.

Table 1: Thermophysical properties of the solid particle and base fluid [12].

Nanoparticle & Base fluid	c_p (J.kg^{-1}.K^{-1})	ρ (kg.m^{-3})	κ (W.m^{-1}.K^{-1})	β (K^{-1})	σ (Sm^{-1})	μ (kg.m^{-1}.s^{-1})	Pr
Solid (TiO_2)	686.2	4250	8.953	0.9×10^{-5}	3.5×10^{6}	-	-
Fluid (H_2O)	4179	997.1	0.613	21×10^{-5}	5.5×10^{-6}	0.001003	6.9

2.4 Governing Equations

The associated governing equations for this 2D steady mixed convective hexagonal heat exchanger nanofluid model with the influence of magnetic field are as follows: [22, 40]:

Continuity Equation:

$$\frac{\partial u}{\partial x} + \frac{\partial v}{\partial y} = 0 \tag{2.1}$$

***X*-momentum Equation:**

$$\rho_{nf}\left(u\frac{\partial u}{\partial x} + v\frac{\partial u}{\partial y}\right) = -\frac{\partial p}{\partial x} + \mu_{nf}\left(\frac{\partial^2 u}{\partial x^2} + \frac{\partial^2 u}{\partial y^2}\right) \tag{2.2}$$

***Y*-momentum Equation:**

$$\rho_{nf}\left(u\frac{\partial v}{\partial x} + v\frac{\partial v}{\partial y}\right) = -\frac{\partial p}{\partial y} + \mu_{nf}\left(\frac{\partial^2 v}{\partial x^2} + \frac{\partial^2 v}{\partial y^2}\right) + g\left(\rho\beta\right)_{nf}\left(T-T_c\right) - \sigma_{nf}B_0^2 v \tag{2.3}$$

Energy Equation:

$$\left(\rho c_p\right)_{nf}\left(u\frac{\partial T}{\partial x} + v\frac{\partial T}{\partial y}\right) = k_{nf}\left(\frac{\partial^2 T}{\partial x^2} + \frac{\partial^2 T}{\partial y^2}\right) \tag{2.4}$$

where p denotes the pressure, g is the acceleration due to gravity, ρ is the density, μ is the dynamic viscosity, β is the thermal expansion coefficient, and T is temperature. Also, the subscript '*nf*' denotes the respective properties of nanofluid.

Moreover, T_c is the reference temperature, σ is the electric conductivity, B_0 is the magnetic field, c_p is the specific heat at constant pressure, k is the thermal conductivity, and u, v are the velocity components along X, Y directions, respectively. In the momentum equation, the external magnetic field and buoyancy force are considered as body force (F), as a result, $g\left(\rho\beta\right)_{nf}\left(T-T_c\right)-\sigma_{nf}B_0^2 v$ is added in the Y-momentum equation. According to this study's formation, the boundary conditions must satisfy each of the followings:

$$
\left.
\begin{aligned}
&u = 0, v = 0, T = T_h \text{ on the left circular surface} \\
&u = 0, v = 0, T = T_c \text{ on the right circular surface} \\
&u = u_0, v = 0, \frac{\partial T}{\partial y} = 0 \text{ on the top horizontal wall} \\
&\text{and } u = v = 0, \frac{\partial T}{\partial n} = 0 \text{ on all other surrounding walls}
\end{aligned}
\right\}
\tag{2.5}
$$

where n is the perpendicular vector acted on the heated surface.

2.5 Properties of Nanofluid

Actually, the thermophysical characteristics of nanofluid are mathematically interrelated with the properties of base fluid (H_2O) and nanoparticles (TiO_2). In general, the following correlations are used to determine the density $\left(\rho_{nf}\right)$, thermal expansion coefficient $\left(\rho\beta\right)_{nf}$, heat capacitance $\left(\rho c_p\right)_{nf}$, and thermal diffusivity of nanofluid $\left(\alpha_{nf}\right)$ [22]:

$$
\rho_{nf} = (1-\phi)\rho_{bf} + \phi\rho_{sp}
\tag{2.6a}
$$

$$
\left(\rho\beta\right)_{nf} = (1-\phi)\left(\rho\beta\right)_{bf} + \phi\left(\rho\beta\right)_{sp}
\tag{2.6b}
$$

$$
\left(\rho c_p\right)_{nf} = (1-\phi)\left(\rho c_p\right)_{bf} + \phi\left(\rho c_p\right)_{sp}
\tag{2.6c}
$$

$$
\alpha_{nf} = \frac{\kappa_{nf}}{\left(\rho c_p\right)_{nf}}
\tag{2.6d}
$$

Moreover, the Brinkman viscosity model [56] is used to calculate the nanofluid's viscosity which is a key property of fluids.

$$\mu_{nf} = \mu_{bf}\left(1-\phi\right)^{-2.5}$$

(2.6e)

Also, the Maxwell-Garnetts model [27, 57] for thermal conductivity of nanofluids, and Maxwell model [28] for electrical conductivity of nanofluids are used to build this mixed convective nanofluid model.

$$\kappa_{nf} = \left\{\frac{k_{sp} + 2k_{bf} - 2\phi\left(k_{bf} - k_{sp}\right)}{k_{sp} + 2k_{bf} + \phi\left(k_{bf} - k_{sp}\right)}\right\}k_{bf}$$

(2.6f)

$$\sigma_{nf} = \left\{1 + \frac{3\left(\frac{\sigma_{sp}}{\sigma_{bf}} - 1\right)\phi}{\left(\frac{\sigma_{sp}}{\sigma_{bf}} + 2\right) - \left(\frac{\sigma_{sp}}{\sigma_{bf}} - 1\right)\phi}\right\}\sigma_{bf}$$

(2.6g)

2.6   Dimensionless Governing Equations

The following non-dimensional governing equations (2.8-2.11) are created, accordingly, by including the dimensionless variables in (2.7) into the dimensional equations (2.1-2.4).

$$\left. X = \frac{x}{L}, Y = \frac{y}{L}, U = \frac{u}{u_0}, V = \frac{v}{u_0}, P = \frac{p}{\rho_{nf}\, u_0^2} \text{ and } \theta = \frac{T - T_c}{T_h - T_c} \right\}$$

(2.7)

The continuity, momentum, and energy equations that result from the dimensionless variables mentioned above are as follows:

$$\frac{\partial U}{\partial X} + \frac{\partial V}{\partial Y} = 0$$

(2.8)

$$U\frac{\partial U}{\partial X} + V\frac{\partial U}{\partial Y} = -\frac{\partial P}{\partial X} + \frac{1}{Re}\left(\frac{\nu_{nf}}{\nu_{bf}}\right)\left(\frac{\partial^2 U}{\partial X^2} + \frac{\partial^2 U}{\partial Y^2}\right)$$

(2.9)

$$U\frac{\partial V}{\partial X}+V\frac{\partial V}{\partial Y}=-\frac{\partial P}{\partial Y}+\frac{1}{\mathrm{Re}}\left(\frac{v_{nf}}{v_{bf}}\right)\left(\frac{\partial^2 V}{\partial X^2}+\frac{\partial^2 V}{\partial Y^2}\right)+\frac{(\rho\beta)_{nf}}{\rho_{nf}\beta_{bf}}Ri\,\theta-\left(\frac{\rho_{bf}\sigma_{nf}}{\rho_{nf}\sigma_{bf}}\right)\frac{Ha^2}{\mathrm{Re}}V \qquad (2.10)$$

$$U\frac{\partial\theta}{\partial X}+V\frac{\partial\theta}{\partial Y}=\left(\frac{\alpha_{nf}}{\alpha_{bf}}\right)\frac{1}{\mathrm{Re}\,\mathrm{Pr}}\left(\frac{\partial^2\theta}{\partial X^2}+\frac{\partial^2\theta}{\partial Y^2}\right) \qquad (2.11)$$

The Reynolds number (*Re*), Prandtl number (*Pr*), Grashof number (*Gr*) and Hartmann number (*Ha*), which are each four different parameters in the equations above that govern this issue, are defined as: $\mathrm{Re}=\dfrac{u_0 L}{\upsilon_{bf}}$, $Pr=\dfrac{\upsilon_{bf}}{\alpha_{bf}}$, $Gr=\dfrac{g\,\beta_{bf}\left(T_h-T_c\right)L^3}{\upsilon_{bf}^2}$, and $Ha=\dfrac{LB_0\sqrt{\sigma_{bf}}}{\sqrt{\mu_{bf}}}$

respectively. Here, $\dfrac{Gr}{\mathrm{Re}^2}=Ri$ is known as Richardson number and $Gr=\dfrac{Ra}{\mathrm{Pr}}$, where

$Ra=\dfrac{g\,\beta_{bf}\left(T_h-T_c\right)L^3}{\upsilon_{bf}\,\alpha_{bf}}$ is known as Rayleigh number. Furthermore, the dimensionless

boundary conditions are:

$$\left.\begin{array}{l} U=V=0,\ \theta=1 \ \text{on the left circular surface}\\[4pt] U=V=0,\ \theta=0 \ \text{on the right circular surface}\\[4pt] U=1,\ V=0,\ \dfrac{\partial\theta}{\partial Y}=0 \ \text{on the top horizontal wall}\\[4pt] \text{and}\ U=V=0,\ \dfrac{\partial\theta}{\partial N}=0 \ \text{on all other surrounding walls} \end{array}\right\} \qquad (2.12)$$

The local Nusselt number (*Nu*$_{loc}$) is defined as:

$$Nu_{loc}=\frac{h.S}{k_{bf}} \qquad (2.13a)$$

where *h*, *k*$_{bf}$ and *S* represent the convective heat transfer rate, thermal conductivity of base fluid, and arc length of heated surface respectively. Also, the convective heat transfer rate from heated surface is obtained form:

$$h=-k_{nf}\left(\frac{\partial\theta}{\partial N}\right)_{\text{heated surface}} \qquad (2.13b)$$

where *N* is the perpendicular vector acted on heated surface.

By using equations (2.13a) and (2.13b), the local Nusselt number along to the cooler surface is calculated by:

$$Nu_{local} = -\frac{k_{nf}}{k_{bf}}\left(\frac{\partial\theta}{\partial N}\right)S \qquad (2.13c)$$

Also, to determine the heat transfer rate from the heated left circular surface to cooler surface the average Nusselt number (Nu_{av}) is calculated by using:

$$Nu_{av} = -\left(\frac{k_{nf}}{k_{bf}}\right)\int_{S}\frac{\partial\theta}{\partial N}dS \qquad (2.14)$$

Here, S represents the surface area of the heated surface. Moreover, ψ denotes the stream function that is connected by $U = \frac{\partial\psi}{\partial Y}$ and $V = -\frac{\partial\psi}{\partial X}$. Furthermore, Ω is the vortices vector that is defined by: $\frac{\partial^2\psi}{\partial X^2} + \frac{\partial^2\psi}{\partial Y^2} = -\left(\frac{\partial V}{\partial X} - \frac{\partial U}{\partial Y}\right) = -\Omega$, where U and V stand for X and Y-axes velocities respectively.

2.7 Finite Element Formulation

Here, the mixed convective heat transfer process is solved using a set of linked nonlinear partial differential equations that are based on the conservation of mass or continuity equation (2.1), conservation of momentum equations (2.2) and (2.3), and conservation of energy equation (2.4). The FEM is a sophisticated numerical method for solving ordinary and partial differential equations that appear in scientific and engineering problems. With this approach, the entire domain is partitioned into smaller, so-called "finite elements," which have finite dimensions. The FEM is an excellent numerical technique for study of scientific and engineering problems. Fluid mechanics, heat transfer, electrical systems, chemical processes, and many other domains use FEM to solve integral equations. Therefore, using the Galerkin weighted residual-based finite element technique, the governing dimensionless equation (2.8) to equation (2.11) with the initial and boundary conditions (2.12) have been numerically solved.

The equations (2.8) -(2.11) are subjected to the weighted residuals Zienkiewicz [52] method to generate the finite element equations as:

$$\int_A N_\alpha \left(\frac{\partial U}{\partial X} + \frac{\partial V}{\partial Y} \right) dA = 0 \tag{2.15}$$

$$\int_A N_\alpha \left(U \frac{\partial U}{\partial X} + V \frac{\partial U}{\partial Y} \right) dA = -\int_A H_\lambda \left(\frac{\partial P}{\partial X} \right) dA + \frac{1}{\text{Re}} \left(\frac{\nu_{nf}}{\nu_{bf}} \right) \int_A N_\alpha \left(\frac{\partial^2 U}{\partial X^2} + \frac{\partial^2 U}{\partial Y^2} \right) dA \tag{2.16}$$

$$\int_A N_\alpha \left(U \frac{\partial V}{\partial X} + V \frac{\partial V}{\partial Y} \right) dA = -\int_A H_\lambda \left(\frac{\partial P}{\partial Y} \right) dA + \frac{1}{\text{Re}} \left(\frac{\nu_{nf}}{\nu_{bf}} \right) \int_A N_\alpha \left(\frac{\partial^2 V}{\partial X^2} + \frac{\partial^2 V}{\partial Y^2} \right) dA$$
$$+ Ri \frac{(\rho\beta)_{nf}}{\rho_{nf} \beta_{bf}} \int_A N_\alpha \theta \, dA - \frac{Ha^2}{\text{Re}} \left(\frac{\rho_{bf} \sigma_{nf}}{\rho_{nf} \sigma_{bf}} \right) \int_A N_\alpha V \, dA \tag{2.17}$$

$$\int_A N_\alpha \left(U \frac{\partial \theta}{\partial X} + V \frac{\partial \theta}{\partial Y} \right) dA = \frac{1}{\text{Re}\,\text{Pr}} \left(\frac{\alpha_{nf}}{\alpha_{bf}} \right) \int_A N_\alpha \left(\frac{\partial^2 \theta}{\partial X^2} + \frac{\partial^2 \theta}{\partial Y^2} \right) dA \tag{2.18}$$

where the element shape functions for the pressure are represented by $H_\lambda \left(\lambda = 1, 2, 3 \right)$ and A is the element area. Also, for the velocity component and temperature, $N_\alpha \left(1, 2, ..., 6 \right)$ represents the element's shape functions or interpolation functions. The velocity components U, V, the temperature θ, and the pressure P are the primary unknowns for the differential equations describing incompressible thermal flow.

In this study, the finite element equations are developed using the six-node triangular element. Only the corner nodes are connected to pressure; the other five nodes are all connected to velocities and temperature. This indicates that a lower order polynomial, which is satisfied by the continuity equation, is chosen for pressure. Equations (2.15) through (2.18) are now subjected to Gauss's theorem in order to produce the boundary integral terms for the surface tractions and heat flux. According to the Gauss's theorem in 2D: $\int_A \nabla . F \, dA = \int_c F . n \, ds$, we have:

$$\int_A \nabla . N_\alpha \nabla U \, dA = \int_c N_\alpha \nabla U . n \, ds \tag{2.19}$$

where $F = N_\alpha \nabla U$.

Again using the vector identity $\nabla.(\phi F) = \phi \nabla.F + \nabla \phi.F$, we can write

$$\nabla.(N_\alpha \nabla U) = N_\alpha \nabla.\nabla U + \nabla N_\alpha.\nabla U \tag{2.20}$$

That is, $\int\limits_A \nabla.(N_\alpha \nabla U) dA = \int\limits_A N_\alpha (\nabla.\nabla U) dA + \int\limits_A \nabla N_\alpha.\nabla U \, dA$

Or, $\int\limits_A N_\alpha (\nabla.\nabla U) dA = \int\limits_A \nabla.(N_\alpha \nabla U) dA - \int\limits_A \nabla N_\alpha.\nabla U \, dA$

Or, $\int\limits_A N_\alpha (\nabla.\nabla U) dA = \int\limits_c N_\alpha \nabla U.n \, ds - \int\limits_A \nabla N_\alpha.\nabla U \, dA$ (by using 2.19) $\tag{2.21}$

Now, with the help of equation (2.21), the equation (2.16) can be written as,

$$\int\limits_A N_\alpha \left(U \frac{\partial U}{\partial X} + V \frac{\partial U}{\partial Y} \right) dA + \int\limits_A H_\lambda \left(\frac{\partial P}{\partial X} \right) dA + \frac{1}{\mathrm{Re}} \left(\frac{\nu_{nf}}{\nu_{bf}} \right) \int\limits_A N_\alpha \left(\frac{\partial N_\alpha}{\partial X} \frac{\partial U}{\partial X} + \frac{\partial N_\alpha}{\partial Y} \frac{\partial U}{\partial Y} \right) dA$$

$$= \frac{1}{\mathrm{Re}} \left(\frac{\nu_{nf}}{\nu_{bf}} \right) \int\limits_{s_0} N_\alpha \, s_x \, ds_0 \tag{2.22}$$

Similarly, the equation (2.16) and (2.17) can be written as,

$$\int\limits_A N_\alpha \left(U \frac{\partial V}{\partial X} + V \frac{\partial V}{\partial Y} \right) dA + \int\limits_A H_\lambda \left(\frac{\partial P}{\partial Y} \right) dA + \frac{1}{\mathrm{Re}} \left(\frac{\nu_{nf}}{\nu_{bf}} \right) \int\limits_A N_\alpha \left(\frac{\partial N_\alpha}{\partial X} \frac{\partial V}{\partial X} + \frac{\partial N_\alpha}{\partial Y} \frac{\partial V}{\partial Y} \right) dA$$

$$- Ri \frac{(\rho\beta)_{nf}}{\rho_{nf}\beta_{bf}} \int\limits_A N_\alpha \theta \, dA + \frac{Ha^2}{\mathrm{Re}} \left(\frac{\rho_{bf}\sigma_{nf}}{\rho_{nf}\sigma_{bf}} \right) \int\limits_A N_\alpha V \, dA = \frac{1}{\mathrm{Re}} \left(\frac{\nu_{nf}}{\nu_{bf}} \right) \int\limits_{s_0} N_\alpha \, s_y \, ds_0 \tag{2.23}$$

$$\int\limits_A N_\alpha \left(U \frac{\partial \theta}{\partial X} + V \frac{\partial \theta}{\partial Y} \right) dA + \frac{1}{\mathrm{Re}\,\mathrm{Pr}} \left(\frac{\alpha_{nf}}{\alpha_{bf}} \right) \int\limits_A N_\alpha \left(\frac{\partial N_\alpha}{\partial X} \frac{\partial \theta}{\partial X} + \frac{\partial N_\alpha}{\partial Y} \frac{\partial \theta}{\partial Y} \right) dA$$

$$= \frac{1}{\mathrm{Re}\,\mathrm{Pr}} \left(\frac{\alpha_{nf}}{\alpha_{bf}} \right) \int\limits_{s_w} N_\alpha \, q_w \, ds_w \tag{2.24}$$

where $s_x = \nabla U.n$ and $s_y = \nabla V.n$ are the surface tractions along outflow boundary s_0.

Also, $q_w = \nabla \theta.n$ is the heat flux that flows into or out from domain along wall boundary s_w

. Here, $(U,V), \theta$ and P are the fundamental unknowns representing velocity components, temperature, and pressure, respectively of the differential equations (2.22)-(2.24).

Now, substitute the element velocity distribution, temperature distribution, pressure distribution and their derivatives. That is,

$$
\left.
\begin{aligned}
U(X,Y) &= N_\beta\, U_\beta \\
V(X,Y) &= N_\beta\, V_\beta \\
\theta(X,Y) &= N_\beta\, \theta_\beta \\
P(X,Y) &= H_\lambda\, P_\lambda
\end{aligned}
\right\}
\tag{2.25}
$$

Also,

$$
\left.
\begin{aligned}
\frac{\partial U}{\partial X} &= N_{\gamma,x}\, U_\gamma, & \frac{\partial U}{\partial Y} &= N_{\gamma,y}\, U_\gamma \\
\frac{\partial V}{\partial X} &= N_{\gamma,x}\, V_\gamma, & \frac{\partial V}{\partial Y} &= N_{\gamma,y}\, V_\gamma \\
\frac{\partial \theta}{\partial X} &= N_{\gamma,x}\, \theta_\gamma, & \frac{\partial \theta}{\partial Y} &= N_{\gamma,y}\, \theta_\gamma \\
\frac{\partial P}{\partial X} &= H_{\delta,x}\, P_\delta, & \frac{\partial P}{\partial Y} &= H_{\delta,y}\, P_\delta
\end{aligned}
\right\}
\tag{2.26}
$$

Now, apply (2.25) and (2.26) into the equations (2.15) and (2.22)-(2.24) one can obtain,

$$
\int_A N_\alpha \left(N_{\gamma,x}\, U_\gamma + N_{\gamma,y}\, V_\gamma \right) dA = 0
\tag{2.27}
$$

$$
\int_A N_\alpha \left(N_\beta\, U_\beta\, N_{\gamma,x}\, U_\gamma + N_\beta\, V_\beta\, N_{\gamma,y}\, U_\gamma \right) dA + \int_A H_\lambda H_{\delta,x}\, P_\delta\, dA
$$

$$
+ \frac{1}{\mathrm{Re}}\left(\frac{\nu_{nf}}{\nu_{bf}} \right) \int_A N_\alpha \left(N_{\alpha,x}\, N_{\gamma,x}\, U_\gamma + N_{\alpha,y}\, N_{\gamma,y}\, U_\gamma \right) dA = \frac{1}{\mathrm{Re}}\left(\frac{\nu_{nf}}{\nu_{bf}} \right) \int_{s_0} N_\alpha\, s_x\, ds_0
\tag{2.28}
$$

$$
\int_A N_\alpha \left(N_\beta\, U_\beta\, N_{\gamma,x}\, V_\gamma + N_\beta\, V_\beta\, N_{\gamma,y}\, V_\gamma \right) dA + \frac{1}{\mathrm{Re}}\left(\frac{\nu_{nf}}{\nu_{bf}} \right) \int_A \left(N_{\alpha,x}\, N_{\gamma,x}\, V_\gamma + N_{\alpha,y}\, N_{\gamma,y}\, V_\gamma \right) dA
$$

$$
+ \int_A H_\lambda H_{\delta,y}\, P_\delta\, dA - Ri\, \frac{(\rho\beta)_{nf}}{\rho_{nf}\beta_{bf}} \int_A N_\alpha\, N_\beta\, \theta_\beta\, dA + \frac{Ha^2}{\mathrm{Re}}\left(\frac{\rho_{bf}\sigma_{nf}}{\rho_{nf}\sigma_{bf}} \right) \int_A N_\alpha\, N_\beta\, V_\beta\, dA +
\tag{2.29}
$$

$$
= \frac{1}{\mathrm{Re}}\left(\frac{\nu_{nf}}{\nu_{bf}} \right) \int_{s_0} N_\alpha\, s_y\, ds_0
$$

$$\int_A N_\alpha \left(N_\beta U_\beta N_{\gamma,x} \theta_\gamma + N_\beta V_\beta N_{\gamma,y} \theta_\gamma \right) dA + \frac{1}{Re}\left(\frac{\alpha_{nf}}{\alpha_{bf}} \right) \int_A N_\alpha \left(N_{\alpha,x} N_{\gamma,x} \theta_\gamma + N_{\alpha,y} N_{\gamma,y} \theta_\gamma \right) dA$$

$$(2.30)$$

$$= \frac{1}{Re}\left(\frac{\alpha_{nf}}{\alpha_{bf}} \right) \int_{s_w} N_\alpha\, q_w\, ds_w$$

Then the finite element equations (2.27)-(2.30) can be written in the form:

$$K_{\alpha\gamma^x} U_\gamma + K_{\alpha\gamma^y} V_\gamma = 0 \tag{2.31}$$

$$K_{\alpha\beta\gamma^x} U_\beta U_\gamma + K_{\alpha\beta\gamma^y} V_\beta U_\gamma + H_{\lambda\delta^x} P_\delta + \left(S_{\alpha^x\gamma^x} + S_{\alpha^y\gamma^y} \right) U_\gamma = Q_{\alpha^u} \tag{2.32}$$

$$K_{\alpha\beta\gamma^x} U_\beta V_\gamma + K_{\alpha\beta\gamma^y} V_\beta V_\gamma + H_{\lambda\delta^y} P_\delta + \left(S_{\alpha^x\gamma^x} + S_{\alpha^y\gamma^y} \right) V_\gamma - K_{\alpha\beta}\theta_\beta + N_{\alpha\beta} V_\beta = Q_{\alpha^v} \tag{2.33}$$

$$K_{\alpha\beta\gamma^x} U_\beta \theta_\gamma + K_{\alpha\beta\gamma^y} V_\beta \theta_\gamma + \left(M_{\alpha^x\beta^x} + M_{\alpha^y\beta^y} \right) \theta_\gamma = Q_{\alpha^\theta} \tag{2.34}$$

where the integrals at the element edges s_o and s_w are the coefficients in the element matrices take the form of:

$$K_{\alpha\gamma^x} = \int_A N_\alpha N_{\gamma,x}\, dA \tag{2.35a}$$

$$K_{\alpha\gamma^y} = \int_A N_\alpha N_{\gamma,y}\, dA \tag{2.35b}$$

$$K_{\alpha\beta\gamma^x} = \int_A N_\alpha N_\beta N_{\gamma,x}\, dA \tag{2.35c}$$

$$K_{\alpha\beta\gamma^y} = \int_A N_\alpha N_\beta N_{\gamma,y}\, dA \tag{2.35d}$$

$$H_{\lambda\delta^x} = \int_A H_\lambda H_{\delta,x}\, dA \tag{2.35e}$$

$$H_{\lambda\delta^y} = \int_A H_\lambda H_{\delta,y}\, dA \tag{2.35f}$$

$$S_{\alpha^x\gamma^x} = \frac{1}{Re}\left(\frac{\nu_{nf}}{\nu_{bf}} \right) \int_A N_{\alpha,x} N_{\gamma,x}\, dA \tag{2.35g}$$

$$S_{\alpha^y\gamma^y} = \frac{1}{Re}\left(\frac{\nu_{nf}}{\nu_{bf}} \right) \int_A N_{\alpha,y} N_{\gamma,y}\, dA \tag{2.35h}$$

$$Q_{\alpha^u} = \frac{1}{\mathrm{Re}} \left(\frac{\nu_{nf}}{\nu_{bf}} \right) \int_{s_0} N_\alpha \, s_x \, ds_0 \tag{2.35i}$$

$$Q_{\alpha^v} = \frac{1}{\mathrm{Re}} \left(\frac{\nu_{nf}}{\nu_{bf}} \right) \int_{s_0} N_\alpha \, s_y \, ds_0 \tag{2.35j}$$

$$Q_{\alpha^\theta} = \frac{1}{\mathrm{Re}\,\mathrm{Pr}} \left(\frac{\alpha_{nf}}{\alpha_{bf}} \right) \int_{s_w} N_\alpha \, q_w \, ds_w \tag{2.35k}$$

$$K_{\alpha\beta} = -\frac{(\rho\beta)_{nf}}{\rho_{nf}\,\beta_{bf}} \, Ri \int_A N_\alpha \, N_\beta \, dA \tag{2.35l}$$

$$N_{\alpha\beta} = \frac{Ha^2}{\mathrm{Re}} \left(\frac{\rho_{bf}\,\sigma_{nf}}{\rho_{nf}\,\sigma_{bf}} \right) \int_A N_\alpha \, N_\beta \, dA \tag{2.35m}$$

$$M_{\alpha^x\gamma^x} = \frac{1}{\mathrm{Re}\,\mathrm{Pr}} \left(\frac{\alpha_{nf}}{\alpha_{bf}} \right) \int_A N_{\alpha,x} \, N_{\gamma,x} \, dA \tag{2.35n}$$

$$M_{\alpha^y\gamma^y} = \frac{1}{\mathrm{Re}\,\mathrm{Pr}} \left(\frac{\alpha_{nf}}{\alpha_{bf}} \right) \int_A N_{\alpha,y} \, N_{\gamma,y} \, dA \tag{2.35o}$$

Nonlinearity exists in the resulting finite element equations (2.31)-(2.34). By first formulating the unbalanced values from the set of the finite element equations (2.31)-(2.34) as follows, the Newton-Raphson iteration approach is used to solve these nonlinear algebraic equations.

$$F_{\alpha^p} = K_{\alpha\gamma^x} U_\gamma + K_{\alpha\gamma^y} V_\gamma \tag{2.36}$$

$$F_{\alpha^u} = K_{\alpha\beta\gamma^x} U_\beta U_\gamma + K_{\alpha\beta\gamma^y} V_\beta U_\gamma + H_{\lambda\delta^x} P_\delta + \left(S_{\alpha^x\gamma^x} + S_{\alpha^y\gamma^y} \right) U_\gamma - Q_{\alpha^u} \tag{2.37}$$

$$F_{\alpha^v} = K_{\alpha\beta\gamma^x} U_\beta V_\gamma + K_{\alpha\beta\gamma^y} V_\beta V_\gamma + H_{\lambda\delta^y} P_\delta + \left(S_{\alpha^x\gamma^x} + S_{\alpha^y\gamma^y} \right) V_\gamma - K_{\alpha\beta}\,\theta_\beta + N_{\alpha\beta} V_\beta - Q_{\alpha^v} \tag{2.38}$$

$$F_{\alpha^\theta} = K_{\alpha\beta\gamma^x} U_\beta \theta_\gamma + K_{\alpha\beta\gamma^y} V_\beta \theta_\gamma + \left(M_{\alpha^x\gamma^x} + M_{\alpha^y\gamma^y} \right) \theta_\gamma - Q_{\alpha^\theta} \tag{2.39}$$

This results in a series of algebraic equations in which the element nodal velocity components, temperatures, and pressures are incremental unknowns in the form:

$$\begin{bmatrix} K_{uu} & K_{uv} & K_{u\theta} & K_{up} \\ K_{vu} & K_{vv} & K_{v\theta} & K_{vp} \\ K_{\theta u} & K_{\theta v} & K_{\theta\theta} & K_{\theta p} \\ K_{pu} & K_{pv} & K_p\theta & K_{pp} \end{bmatrix} \begin{bmatrix} \Delta u \\ \Delta v \\ \Delta\theta \\ \Delta p \end{bmatrix} = - \begin{bmatrix} F_{\alpha^u} \\ F_{\alpha^v} \\ F_{\alpha^\theta} \\ F_{\alpha^p} \end{bmatrix} \qquad (2.40)$$

where,

$$K_{uu} = K_{\alpha\beta\gamma^x} U_\gamma + K_{\alpha\beta\gamma^x} U_\beta + K_{\alpha\beta\gamma^y} V_\beta + \left(S_{\alpha^x\beta^x} + S_{\alpha^y\beta^y} \right) \qquad (2.41a)$$

$$K_{uv} = K_{\alpha\beta\gamma^y} U_\gamma \qquad (2.41b)$$

$$K_{up} = H_{\lambda\delta^x} \qquad (2.41c)$$

$$K_{vu} = K_{\alpha\beta\gamma^x} V_\gamma \qquad (2.41d)$$

$$K_{vv} = K_{\alpha\beta\gamma^x} U_\beta + K_{\alpha\beta\gamma^y} V_\gamma + K_{\alpha\beta\gamma^y} V_\beta + \left(S_{\alpha^x\beta^x} + S_{\alpha^y\beta^y} \right) + N_{\alpha\beta} \qquad (2.41e)$$

$$K_{v\theta} = -K_{\alpha\beta} \qquad (2.41f)$$

$$K_{vp} = H_{\lambda\delta^y} \qquad (2.41g)$$

$$K_{\theta u} = K_{\alpha\beta\gamma^x} \theta_\gamma \qquad (2.41h)$$

$$K_{\theta v} = K_{\alpha\beta\gamma^y} \theta_\gamma \qquad (2.41i)$$

$$K_{\theta\theta} = K_{\alpha\beta\gamma^x} U_\beta + K_{\alpha\beta\gamma^y} V_\beta + \left(M_{\alpha^x\gamma^x} + M_{\alpha^y\gamma^y} \right) \theta_\gamma \qquad (2.41j)$$

$$K_{pu} = K_{\alpha\gamma^x} \qquad (2.41k)$$

$$K_{pv} = K_{\alpha\gamma^y} \qquad (2.41l)$$

and $K_{u\theta} = K_{\theta p} = K_{p\theta} = K_{pp} = 0$ \qquad (2.41m)

If the percentage of the overall change from previous iteration is less than the given value, the iteration process ends. In MATLAB, a set of global nonlinear algebraic equations is produced using Newton-Raphson iteration approach that can be used to solve these governing equations. The convergence condition for this weighted residual approach is established such that $\left| \Gamma^{m+1} - \Gamma^m \right| < 10^{-5}$ for any variables that is not as important where $m+1$ and m represent two repetitions in succession, and $\Gamma(U,V,\theta)$ stands for the iteration's values.

2.8   Computational Procedure

The dimensionless governing equations (2.8)-(2.11), including boundary conditions (2.12), are used for the numerical calculations. Also, the hexagonal enclosure has been discretized into multiple triangle-shaped parts. These governing equations are numerically solved with the aid of the finite element Galerkin weighted residual method [9]. In order to measure the thermal performance and the motion of fluid, the whole territory is partitioned into non-overlapping triangular form elements, which requires six nodes and takes into account quadratic interpolation functions. Six nodes are used in the current inquiry, and triangle-shaped components from those nodes are used to improve finite element equations where velocity and temperature are coupled to all six nodes. Only pressure is connected to the nodes in the corner. Between momentum equations for the continuity requirement and a shape function of lower order chosen for the pressure that is satisfied by the continuity equation, the matching of the pressure gradient has occurred. Additionally, to calculate pressure gradient the linear interpolation algorithm is occupied.
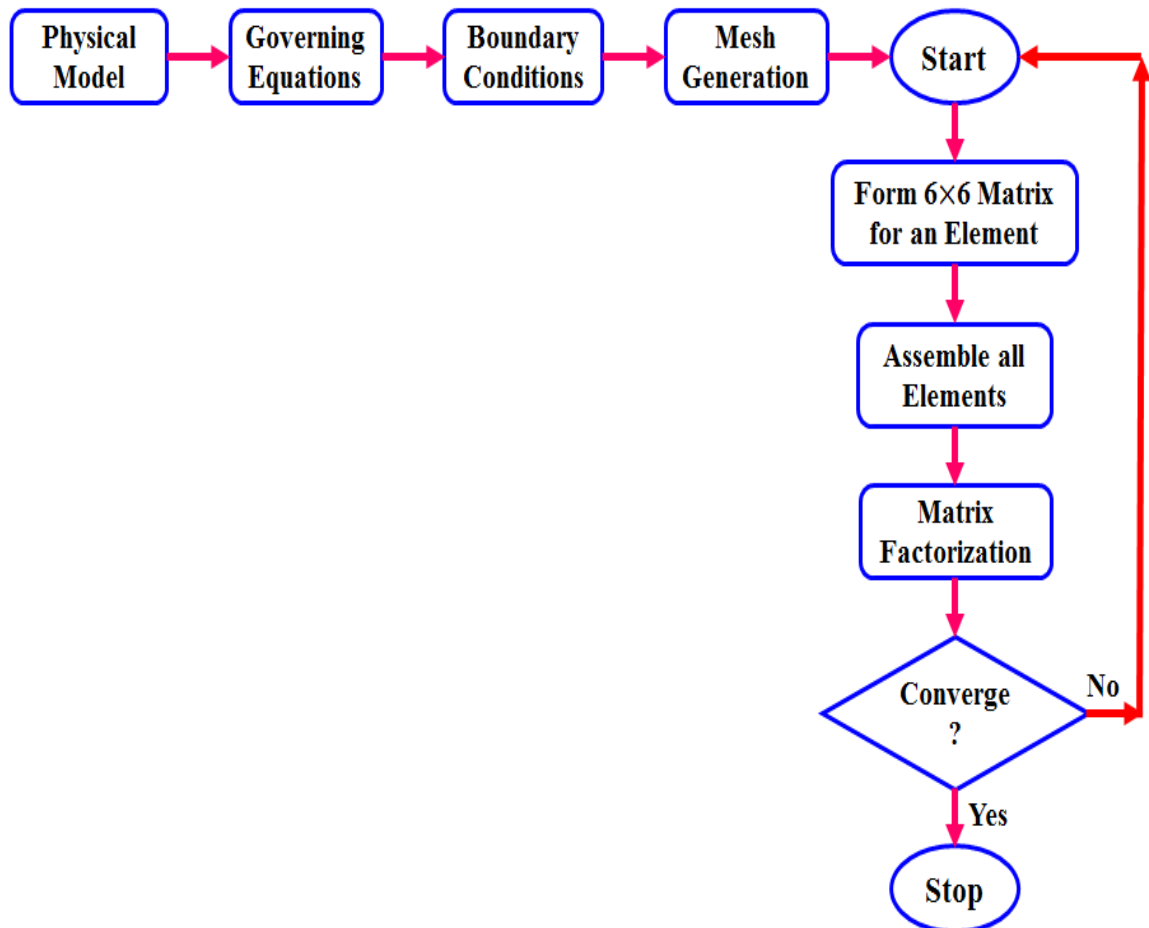

Figure 2.3: A complete flow chart of the computational procedure.

Furthermore, each element's dependent variables are roughly represented as local element coordinates by the involvement of interpolation functions. In this thesis work, to understand the finite element technique, all necessary calculations are performed in section 2.7 over the dimensionless governing equations (2.8)-(2.11) and the non-dimensional boundary conditions (2.12). While it is non-continuous between the elements, the same pressure is taken into account with linear elements. The governing non-linear partial differential equations are then given the Galerkin weighted residual approach, which converts the non-linear partial differential governing equations into a system of integral equations. These equations' integral components are solved using Gauss' quadrature method. The non-linear algebraic equations are then modified by boundary conditions as well. If the overall change percentage from the previous iteration is less than the stated value, the iteration process comes to an end. The Figure 2.3 depicts the entire flowchart of this computing process by finite element method.

2.9 Mesh Generation

In finite element method (FEM), the approach to partition a domain into a collection of subdomains is known as mesh generation or grid generation. Mesh cells are used to discretize a local approximation from a vast domain. The objective is to produce a mesh with high-quality (well-shaped) cells that precisely represents the input domain geometry while not having an excessive number of cells that would make further calculations impossible. The mesh should also have fine (tiny elements) elements in locations that are crucial for the calculations that follow. Meshes are utilized for physical simulations like FEM or CFD as well as for rendering to a computer screen. In Figure 2.4, a hexagonal domain is shown separated into a number of subdomains by triangular elements. But, tetrahedral, pyramids, prisms, or hexahedra must be used for building 3D meshes for finite element analysis. By using the Delaunay triangular method, the current numerical strategy will discretize the computational domain into unstructured triangles. Among all feasible triangulations of a vertex set in 2D, the Delaunay triangulation maximizes the smallest angle.
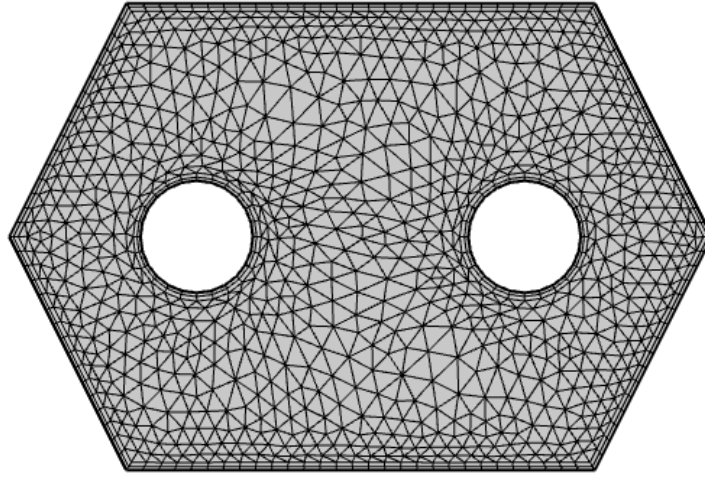
Figure 2.4: Discretization for finite element method of a domain.

2.10 Grid Independence Analysis

A grid sensitivity assessment is described in order to procure the ideal number of elements for this finite element scheme. For using the finite element approach, the entire domain for this fluid model is discretized into five distinct numbers of triangle elements these are 2094, 3372, 8878, 24600 and 32618 respectively. To test the grid independence two different cases are used, where case 1 for $Re = 10$, $Ha =100$ and $\phi = 0$, and case 2 for $Re = 200$, $Ha =0$ and $\phi = 0.1$. For both cases $Ri =1$ and $Pr = 6.9$ are taken as fixed.

Again, to perform this independency test for mesh generation, the optimum value of the average Nusselt number (Nu_{av}) is chosen. In Table 2, the computational outcomes of Nu_{av} for various numbers of triangle elements of this hexagonal cavity are shown.

Table 2: Grid independency analysis for present study.

	Number of Triangular Elements				
	2094	3372	8878	24600	32618
Nu_{av} (case 1)	1.7832	1.8080	1.8940	1.9222	1.9222
Nu_{av} (case 2)	12.113	12.307	12.755	12.830	12.830
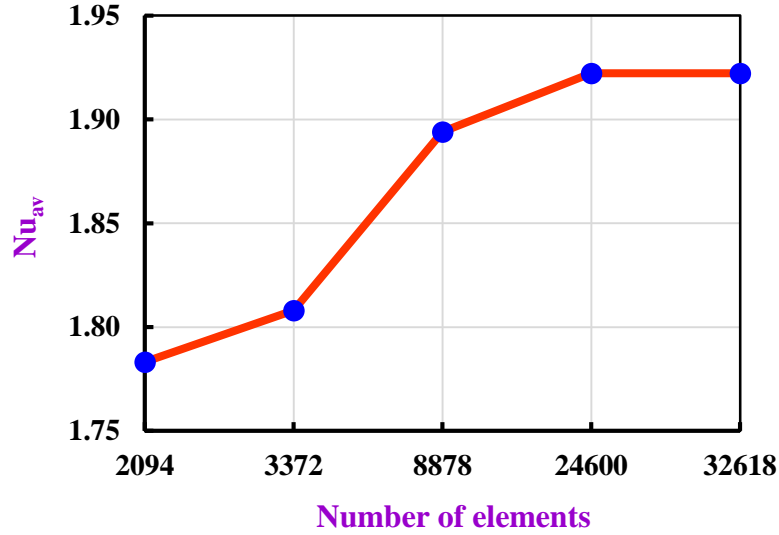
Figure 2.5: Grid sensitivity test by Nu_{av} for $Ri = 1$, $Re = 10$, $Ha = 100$, and $\phi = 0$.
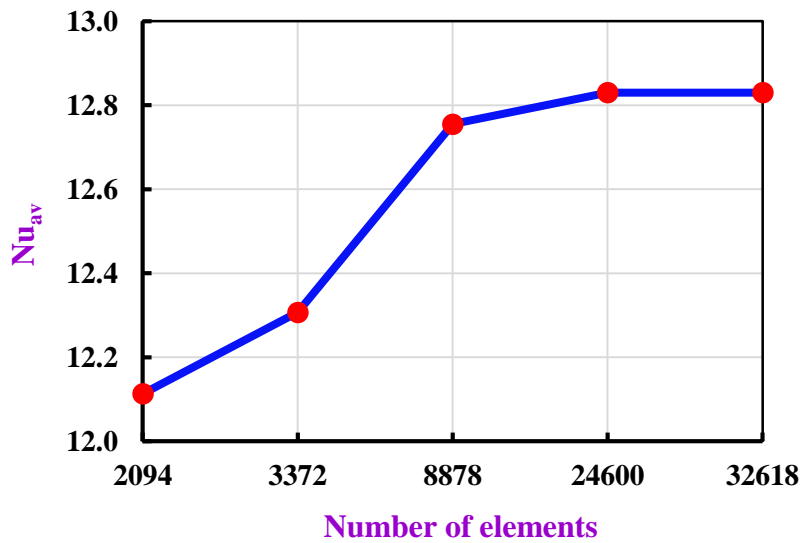
Figure 2.6: Grid sensitivity test by Nu_{av} for $Ri = 1$, $Re = 200$, $Ha = 0$, and $\phi = 0.1$.

Also, the Figure 2.5 and Figure 2.6 demonstrate line graphs of the values of Nu_{av} for different number of elements. These two figures and Table 2 exhibit that for the 24600 triangular elements, for both cases, the values of Nu_{av} are essentially the same to those found for the subsequent higher triangular elements. As a result, in order to solve this heat exchanger fluid flow model, the 24600 triangular elements is chosen for discretization.

2.11 Code Validation

In this section, isotherm lines with streamlines are operated to evaluate the authenticity of this study with the work of Sivakumar et al. [58] that was a lid driven mixed convection analysis. Sivakumar's results are compared to the current findings for a proper agreement about this lid driven mixed convection heat exchanger model. They made a square arena by absorbing some heat on the left side and lid velocity on the upper wall where $Ri = 0.01$, $Pr = 0.71$, and $Re = 100$ were consider in that simulation. Moreover, in this work, the authors are simulated the work of Sivakumar's et al. [58], and compared with the isotherm lines as well as streamlines (in Figure 2.7). The top two are the results of Sivakumar's work, and the bottoms two are from the present investigation.
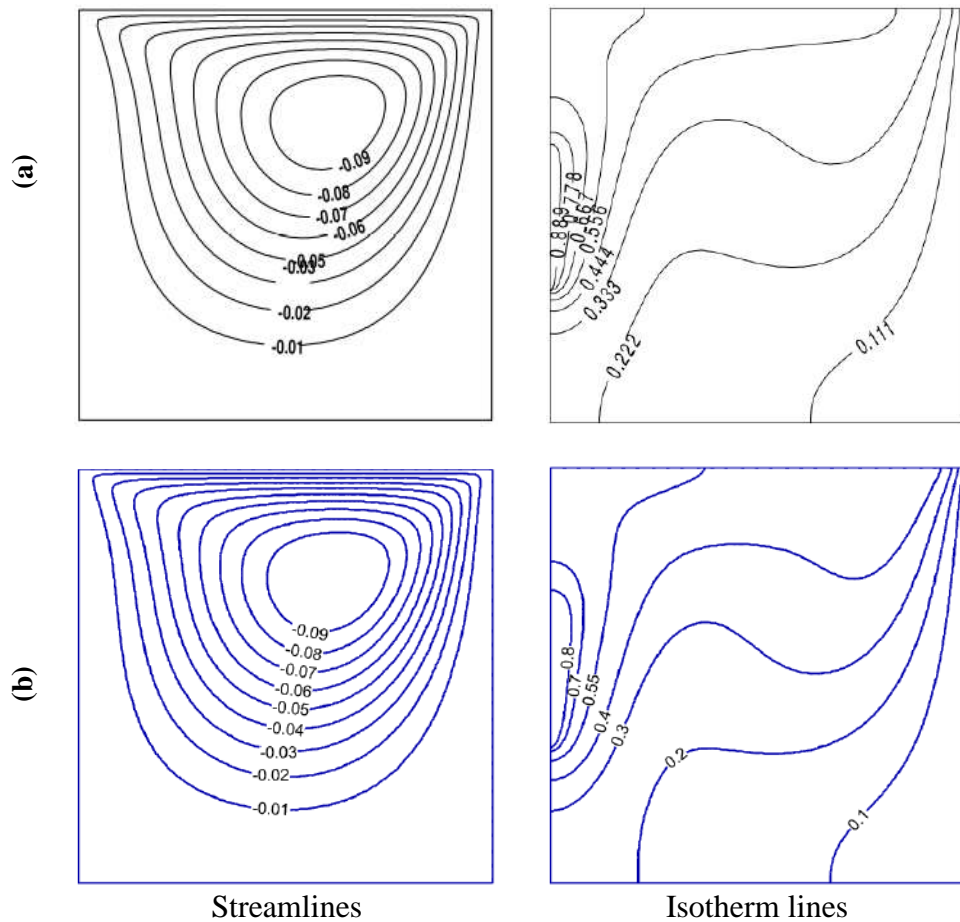
Figure 2.7: Comparison of streamlines and isotherm lines: (a) Sivakumar et al. [58]; (b) present code.
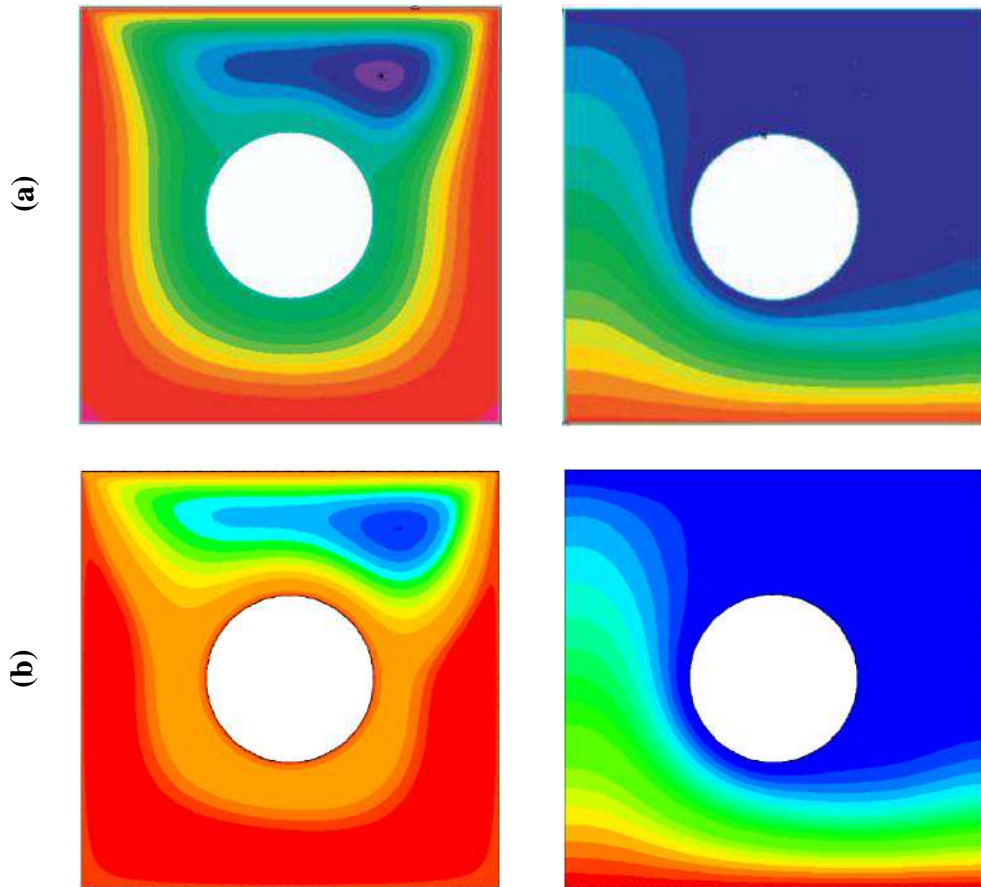
Figure 2.8: Comparison of streamlines and isotherm lines: (a) Khanafer et al. [59]; (b) present code.

Another validation from Khanafer et al. [59] is used to prove the authenticity of current work. They took a lid-driven square arena with rotating cylinder where $Ri = 0.01$, $Pr = 0.7$, and $Re = 100$. The top two are the results of Khanafer's work, and bottoms two are from present study. The streamline and isotherm shape closely resemble this current result. These two results based on lid-driven mixed convective enclosure demonstrate good agreement with the current numerical study, which raises our level of confidence in this mixed convective within close cavity.

CHAPTER 3

Results and Discussion

In this section, engineering-focused simulations of physical variables for mixed convective nanofluid flow inside a hexagonal-shaped heat exchanger with the consequence of magnetic field have been discussed. Within this cavity, streamline and isotherm contours are used to explain the outcomes that are obtained. The hexagonal cavity is filled by TiO_2-H_2O nanofluid where TiO_2 nanoparticles are used as uniform spherical shape. The Figures 3.1-3.21 are used to illustrate how this heat exchanger model is affected by the crucial variables like Hartmann number (Ha), Richardson factor (Ri), Reynolds parameter (Re) and nanoparticle volume fraction (ϕ). Also, the heat exchanger's enactment for nanofluid as well as for water is explained through the use of Nu_{av}. Furthermore, the response surface method (RSM) is applied for stability analysis of response function (Nu_{av}) with respect to input factors Re, Ha and ϕ. Moreover, ANOVA test is performed and analyzed in details for getting a proper regression equation of dependent and independent factors. The standard values for these key parameters that are considered to fulfill this work are $\phi = 0.04$, $Ri = 1$, $Ha = 10$, and $Re = 100$.

3.1 Influence of Reynolds number

In Figure 3.1-3.2, the result of Reynolds number (Re) on heat transportation and fluid motion is exposed by streamline and isotherm contours for this mixed convection model. The Figure 3.1(a) explains the control of Re (10-200) on velocity field of fluid using streamline contours when $Ri = 1$, $Ha = 10$, $Pr = 6.9$, and $\phi = 0.04$. Physically, the higher values of Re rises the fluid inertia, as a result, streamline concentration and flow circulation magnitude rise noticeably. Also, the intensification of Re indicates the rise of inertia forces of the top wall of the hexagonal cavity, the movement of fluid flow goes along to the upper wall from the left to the right with lid velocity. This movement of fluid flow from left to right along the upper surface are increasing with the upsurge of Re, which is the maximum for $Re = 200$. A small vorticity is also noticed at the bottom-right corner of this enclosure. That is, with the development of Re, the fluid velocity (along Y-axis) complete the full domain is becoming upsurge which is represented by Figure 3.2.

On the other hand, the control of *Re* on fluid temperature by isotherm contours is explained in Figure 3.1(b) that demonstrates the improvement in heat transfer in the fluid domain with the increasing of *Re*. At low value of *Re* (10), the existence of natural convection is noticeable. Consequently, the isotherm lines shift uniformly from the left hot cylinder to the right cooler one. With the rise of *Re* (50), the lid velocity is increased, and force convection occurred due to the rise of lid velocity of the higher wall.
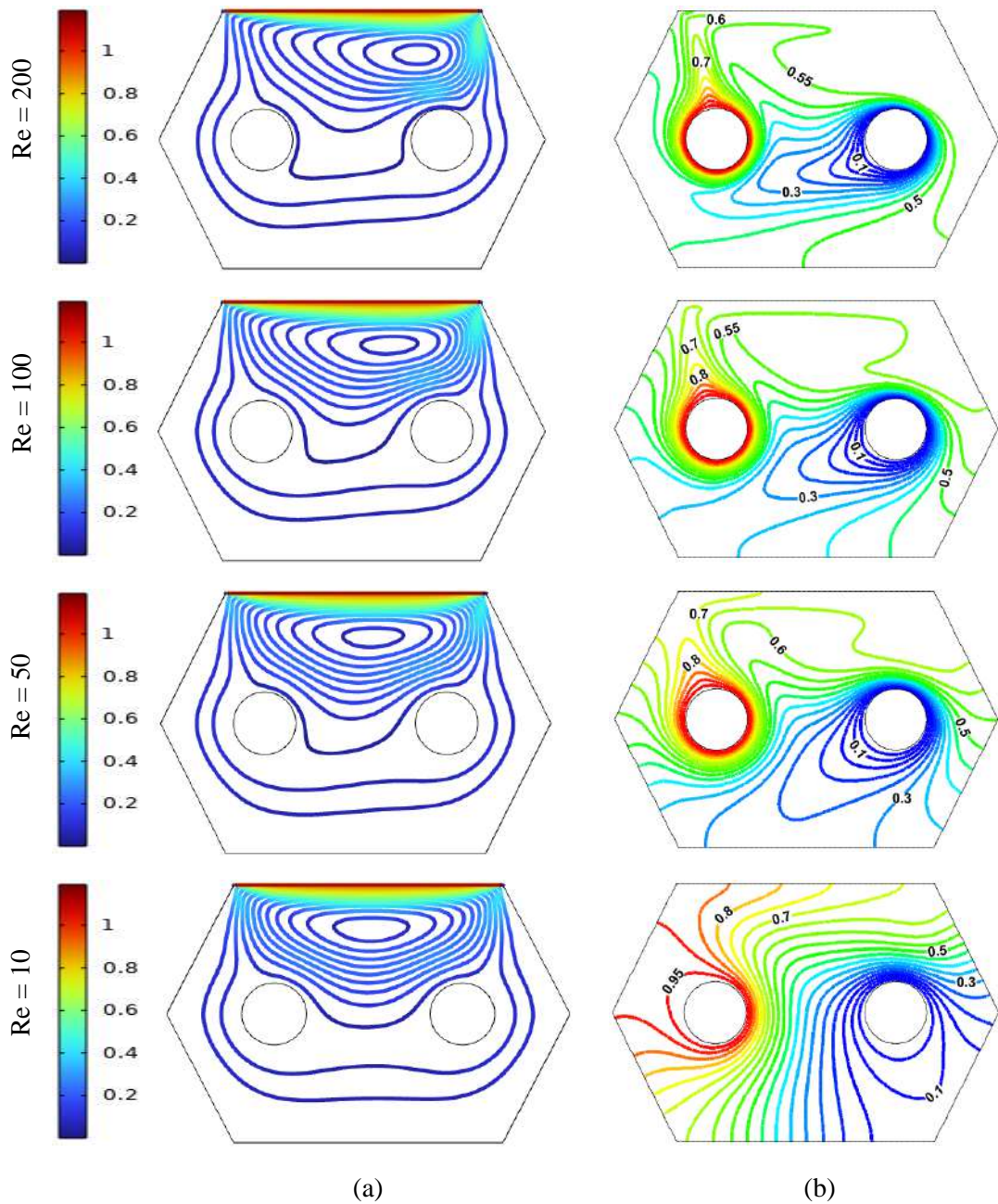

(a)   (b)

Figure 3.1. Influence of *Re* on: (a) streamlines; (b) isotherms contours.

As a result, the heat transfer rate is increased by 82.51% than the previous. So, the red color contour lines that represents the high temperature moves to the cooler surface with the fluid movement. Also for improving the Reynolds number from 50 to 100, the heat transfer rate from the hot surface is 35.43%. Finally, for $Re = 200$, this rate is 23.06%. That is, the rate of heat transportation is improved through the intensification of Re.
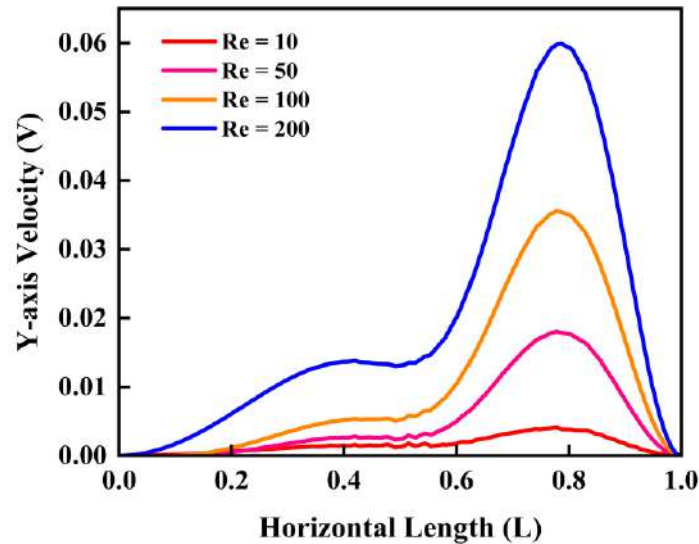
Figure 3.2. Influence of Re on velocity field.

3.2 Influence of Richardson number

The influence of Richardson number (Ri) is illustrated in Figure 3.3-3.5 by involving streamline and isotherm contours along with fluid velocity and Nu_{av}. The changing value of Ri affects the fluid flow pattern which is clearly noticeable in Figure 3.3(a). Firstly, take a look at the mixed convection mode (for $Ri = 1$) when the buoyancy and inertia forces are in balance. As a result, the central vortex has a moving effect along the upper lid wall. Also, the effect of natural convection flow is clear from the uniform streamlines. Secondly, when the value of Ri is become increasing, the vortex turns into wider in the streamlines. The physical interpretation is that the increasing value of Ri indicates the dominance of natural convection that improve the shear stresses. As a result, this produced shear stresses gives resistance to fluid motion. That means, growing value of Ri decreases the fluid velocity which is represented in Figure 3.4.

Conversely, when the magnitude of *Ri* goes to 0.1 and 0.01 from 1, the mode of mixed convection turns to force convection. Due to this, the streamlines are slightly moved to the lid wall. Alternatively, the isotherm lines in Figure 3.3(b) and the *Nu*$_{av}$ in Figure 3.5 demonstrate that the rate of thermal transportation is enlarged with rising *Ri* values, which is analogous to the work of Toudja et al. [42]. When *Ri* goes to 1 to 10, the average heat transfer rate (*Nu*$_{av}$) is enlarged by 17.94%.

(a)   (b)
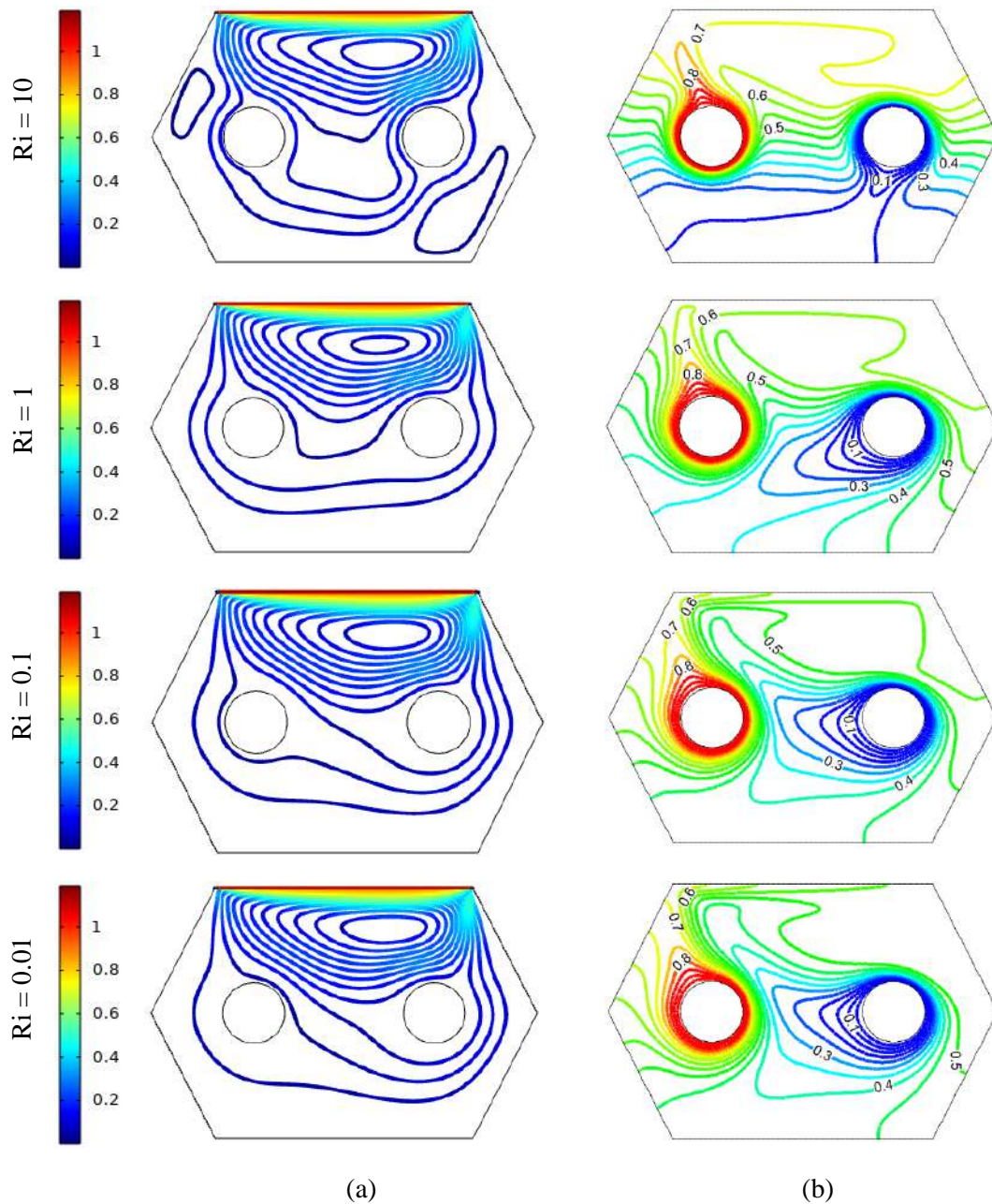
Figure 3.3. Influence of *Ri* on: (a) streamlines; (b) isotherms contours.
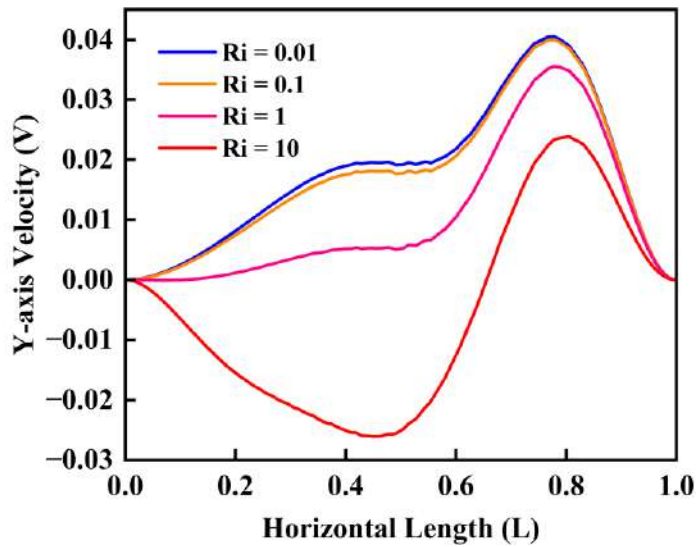
Figure 3.4. Influence of *Ri* on velocity field.
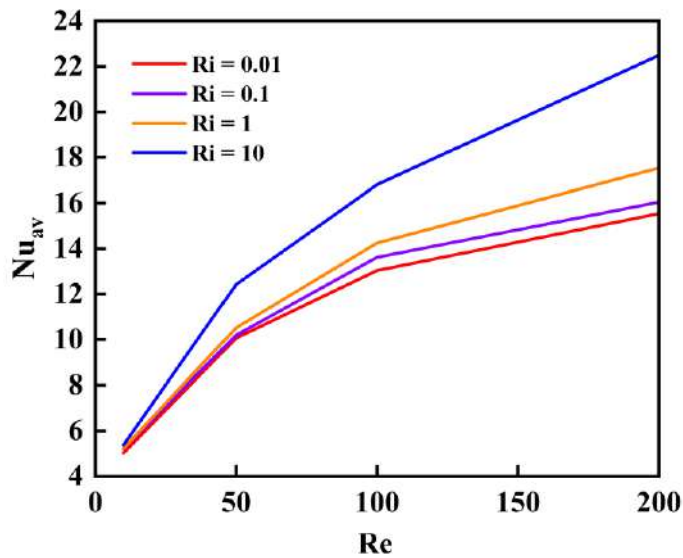
Figure 3.5. Influence of *Ri* on *Nu_{av}*.

Moreover, the average heat transfer rate (for different values of *Re* and *Ri*) from the left hot cylinder (Nu_{source}) which is acted as heat source to the right cylinder is expressed by Table 3. Also, the average heat acceptance rate from the right cold cylinder (Nu_{sink}) which is acted as heat sink is also expressed by Table 3. Since all other surrounding walls are adiabatic, so the value of Nu_{source} and Nu_{sink} will be very close. Also, there occurs a little difference between these two that is expressed by absolute percentage error. These error is very low. This low error expresses that this heat exchanger model is also sufficient to transfer heat from hot surface to cooler on.

Table 3: Heat transfer and acceptance rate from hot and cold surface by *Re* and *Ri*.

	Re	*Nu*$_{source}$	*Nu*$_{sink}$	Absolute % error
Ri = 0.01	10	3.2126	3.2428	0.94
	50	6.4996	6.5831	1.28
	100	7.6378	7.827	2.47
	200	8.2386	8.6653	5.17
Ri = 0.1	10	3.2203	3.2505	0.93
	50	6.5694	6.6479	1.19
	100	7.8187	7.986	2.13
	200	8.6062	8.9582	4.09
Ri = 1	10	3.2997	3.3285	0.87
	50	6.9957	7.032	0.51
	100	8.8291	8.84	0.12
	200	15.262	15.167	0.84
Ri = 10	10	4.0439	4.0581	0.35
	50	9.0028	8.8785	1.38
	100	12.379	11.855	4.23
	200	21.421	21.28	0.65

3.3 Influence of Hartmann number

In Figure 3.6-3.7, the outcome of Hartmann variable (*Ha*) on thermal transportation and fluid motion are showed by streamline, isotherm and heatline contours when *Ri* = 1, *Re* = 100, *Pr* = 6.9, and ϕ = 0.04. Actually, *Ha* portrays the control of magnetic force on this hexagonal heat exchanger. The density of streamlines is maximum when the magnetic field is not active (that is *Ha* = 0), as can be seen in Figure 3.6(a). However, as the magnetic field intensifies (*Ha* = 25), the strength of the flow circulation inside the enclosure slows down.

Moreover, in absence of magnetic force (*Ha* = 0), the fluid movement is maximum rather than the existence of magnetic field (*Ha* = 25, 50, 100). With the increasing of *Ha*, the fluid movement is becoming slower. As a consequence, convection form of heat transport gradually gives way to conduction mode, and the isotherm lines are being to uniform shape along vertical direction. A resistive force named Lorentz force, which has a liability to reduce the speed of the nanofluid's motion inside the enclosure, is active resulting from the magnetic force effect. This is the physical reasons behind this phenomenon. So, the streamlines are nearly close to the top lid surface.
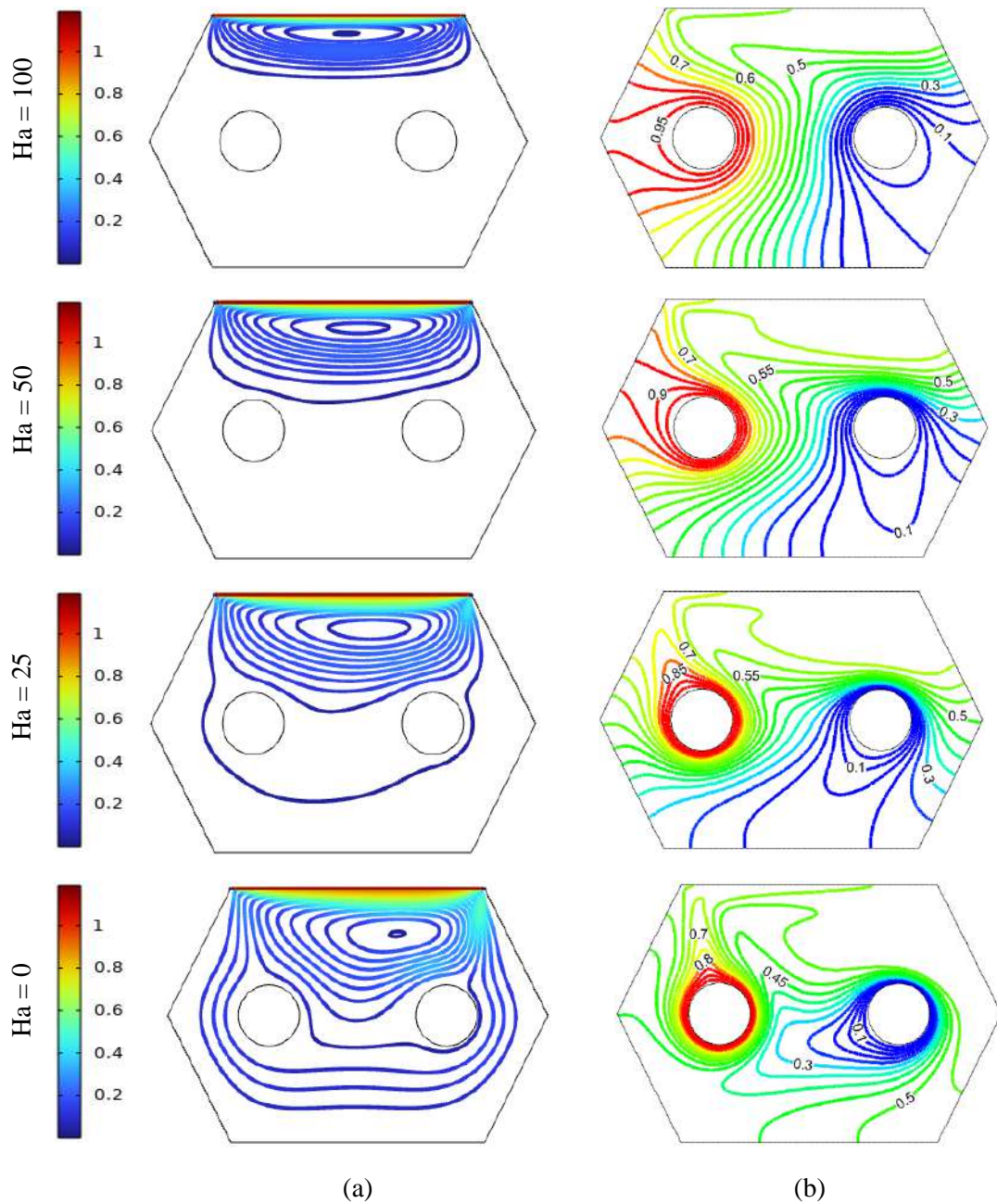
Figure 3.6. Influence of *Ha* on: (a) streamlines; (b) isotherms contours.

Furthermore, the fluid velocity is also a decreasing function of *Ha* that is represented in Figure 3.7. In addition, as *Ha* increased, the temperature field changed slightly which is illustrated by isotherm lines in Figure 3.6(b). When the magnetic effect is inactive (*Ha* = 0), the heat transfer rate (Nu_{av}) is maximum. For *Ha* = 25, the Nu_{av} is decreased at 32.52%. From changing the *Ha* number 25 to 50, this diminishing rate is 30.43%. Also, for highest value of magnetic effect (*Ha* = 100), this reducing rate is 19.76%.
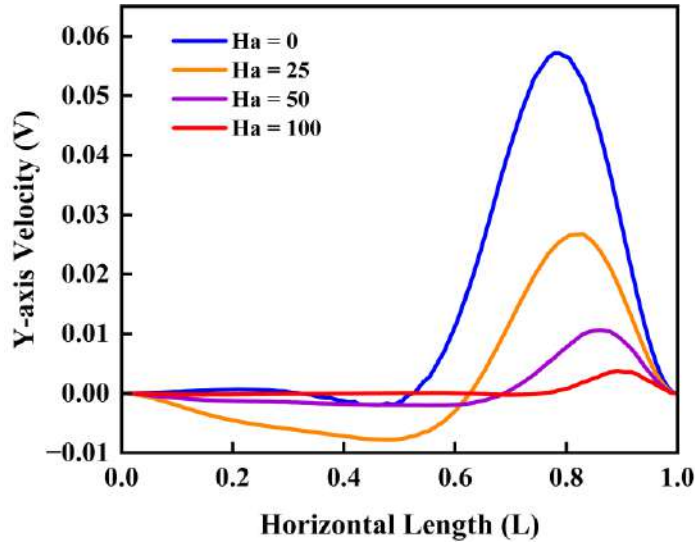
Figure 3.7. Influence of *Ha* on velocity field.

3.4 Influence of Nanoparticle Volume Fraction

In this section, Figure 3.8-3.12 is used to describe the nature of fluid motion and heat transport on current heat exchanger model for dissimilar values of nanoparticle volume fraction (ϕ). When nanoparticles are included to the base fluid, the particles' motion on this fluid domain faces resistance. The fluid's inertia force is amplified by adding nanoparticles because they increase the fluid's overall mass in the cavity. Due to the increasing inertia force, the fluid flow begins to slightly slow down.

Another aspect is that adding more nanoparticles makes the solution more viscous, and particle-particle interactions in this solution inside the enclosure are insignificant. As a result, the streamline contours which expressed in the Figure 3.8(a) represent that the fluid movement along the cavity is being minimized with the adding nanoparticle volume fraction. Also, the fluid velocity along *Y*-axis is being decreased with the rise of ϕ which is clear from the Figure 3.9 (zoom view) at $Ri = 1$, $Re = 100$, and $Ha = 10$. Though the changes of fluid motion are very small but the changes of heat transfer rate are clearly seen in by using isotherm contours in the Figure 3.8(b). The heat exchanger's heat transfer rate (Nu_{av}) is being increased through the intensification of ϕ which is explained by Figure 3.10. The line graph in Figure 3.10(a) expresses that without nanoparticle ($\phi = 0$) the heat transportation rate is minimum compared to the existence of nanoparticles, and for $\phi = 0.01$ and 0.04, the Nu_{av} is uniformly developed. Also, Nu_{av} is maximum when the size of nanoparticles is increased by 10% ($\phi = 0.1$).
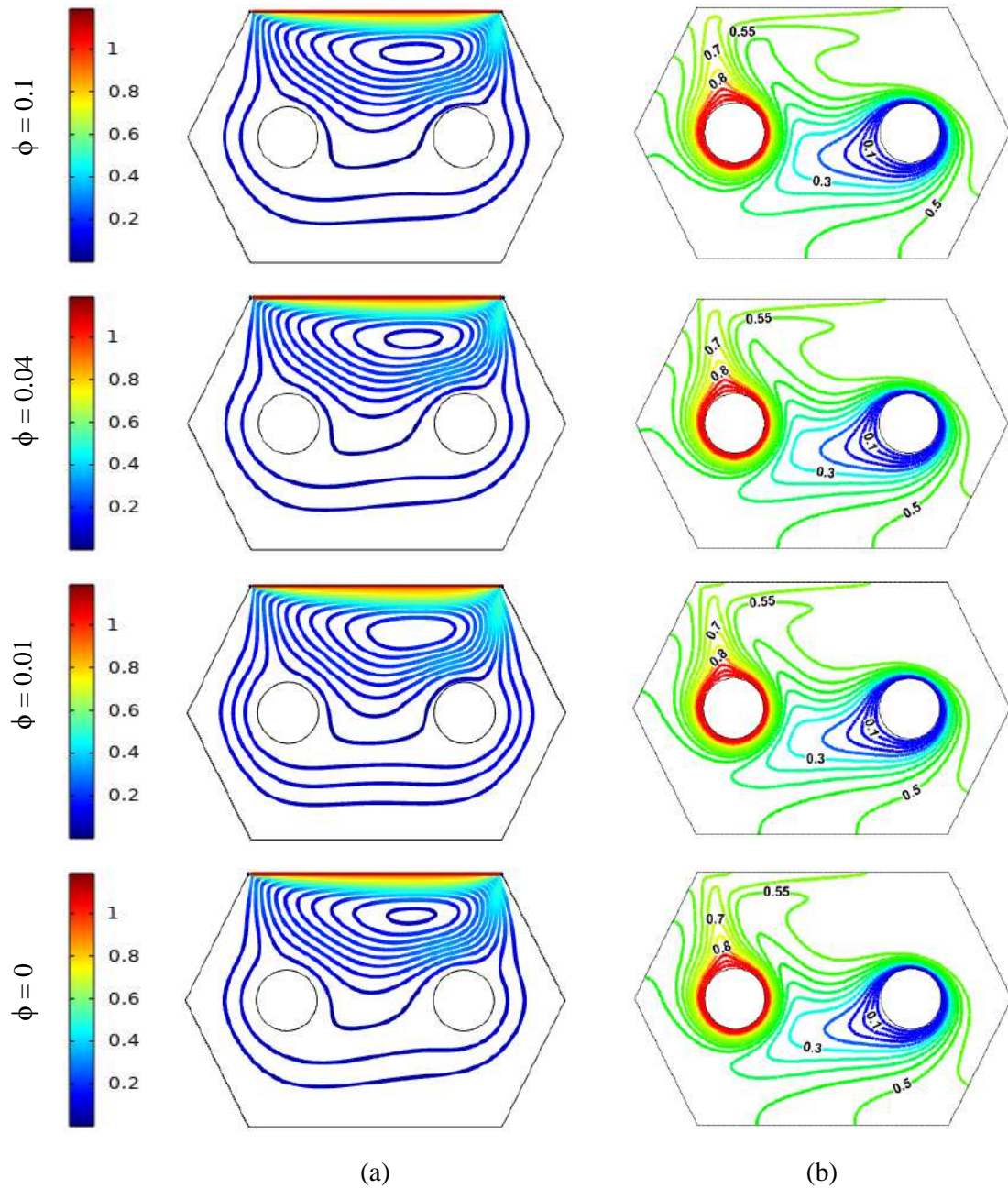
Figure 3.8. Influence of ϕ on: (a) streamlines; (b) isotherms contours.

Furthermore, when the ϕ is increased by 10% ($\phi = 0.1$), the Nu_{av} is significantly developed by 17.69% compared to $\phi = 0$. The physical reason of this occurrences is that the thermal conductivity of nanofluid of entire enclosure rises for the greater size of nanoparticles. The physical reason of this occurrence is that the thermal conductivity of nanofluid of entire enclosure rises for the greater size of nanoparticles. Moreover, Figure 3.10(b) represents a 2D contour plot to visualize Nu_{av} due to change of ϕ and Re. This also indicates the same effect for developing the size of nanoparticles into the water on this heat exchanger.
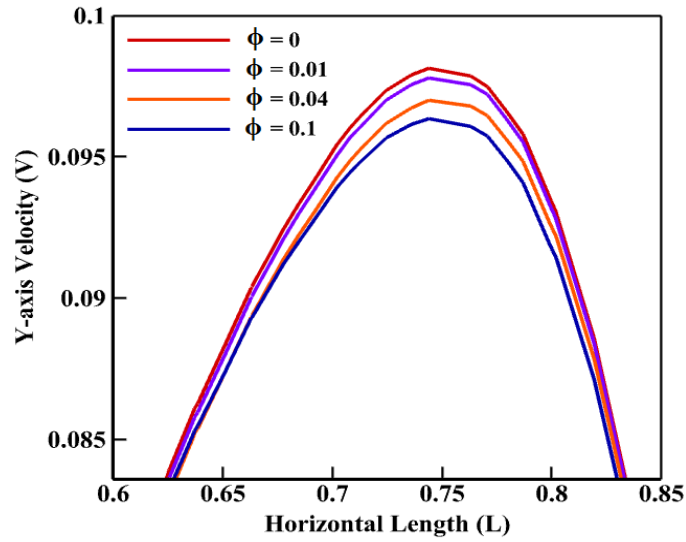
Figure 3.9. Influence of ϕ on velocity field.

| (a) | (b) |
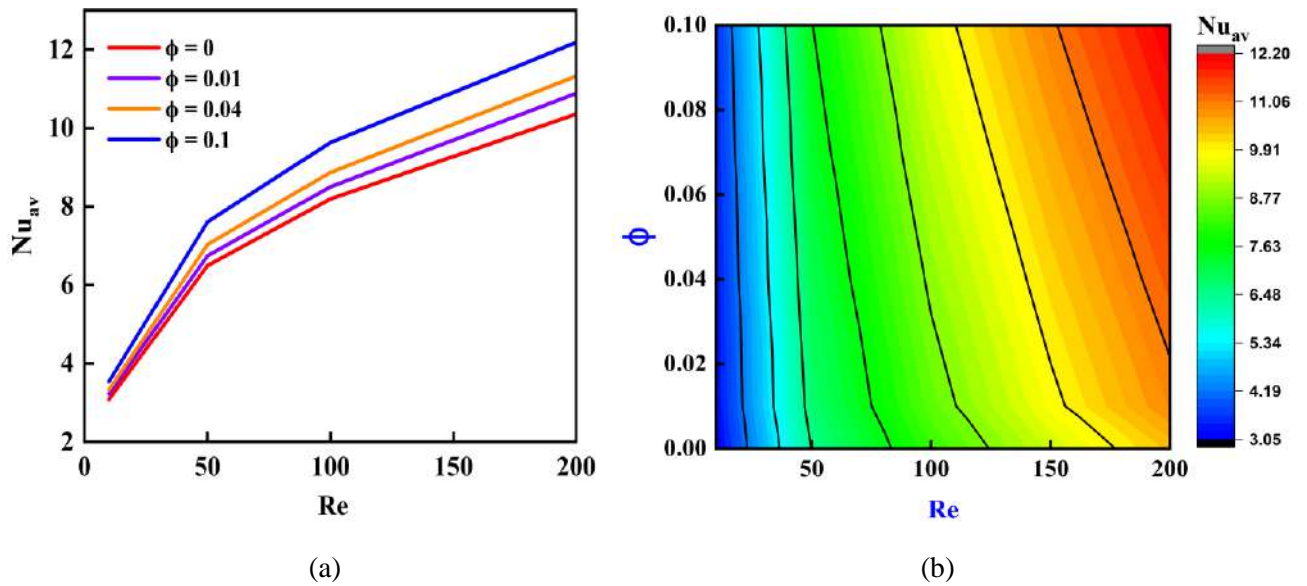
Figure 3.10: Influence of ϕ and *Re* on *Nu*$_{av}$: (a) 2D line graph; (b) 2D contour plot.

On the other hand, the impact of ϕ with the changes of *Ri* are depicted in Figure 3.11 in two different perspectives. For low values of *Ri* and absence of nanoparticles ($\phi = 0$), the *Nu*$_{av}$ is comparatively low than the existence of nanoparticles into water. The line graph in Figure 3.11(a) indicates that *Nu*$_{av}$ is maximum for rising the size of nanoparticles as 10% ($\phi = 0.1$) with *Ri* = 10. Similar impact is noticeable from the 2D contour plot in Figure 3.11(b). Finally, the Figures 3.12(a) express the important of adding nanoparticles into base fluid for this mixed convective hexagonal heat exchanger MHD nanofluid model.

Moreover, the average heat transfer rate (for different values of Re and ϕ) from the left hot cylinder (Nu_{source}) which is acted as heat source to the right cylinder is expressed by Table 4. Also, the average heat acceptance rate from the right cold cylinder (Nu_{sink}) which is acted as heat sink. There occurs a little difference between these two that is expressed by absolute percentage error, but these error is very low.

Table 4: Heat transfer and acceptance rate from hot and cold surface by Re and ϕ.

	Re	Nu_{source}	Nu_{sink}	Absolute % Error
$\phi = 0$	10	3.0794	3.1689	2.91
	50	6.4937	6.5684	1.15
	100	8.1928	8.1415	0.63
	200	10.356	10.067	2.79
$\phi = 0.01$	10	3.2257	3.2384	0.39
	50	6.744	6.7603	0.24
	100	8.5018	8.5049	0.04
	200	10.886	10.828	0.53
$\phi = 0.04$	10	3.3246	3.3382	0.41
	50	7.0322	7.0511	0.27
	100	8.8701	8.8793	0.10
	200	11.326	11.277	0.43
$\phi = 0.1$	10	3.539	3.5546	0.44
	50	7.6076	7.6313	0.31
	100	9.6333	9.6549	0.22
	200	12.189	12.164	0.21

(a)　　　　　　　　　　　　　　(b)
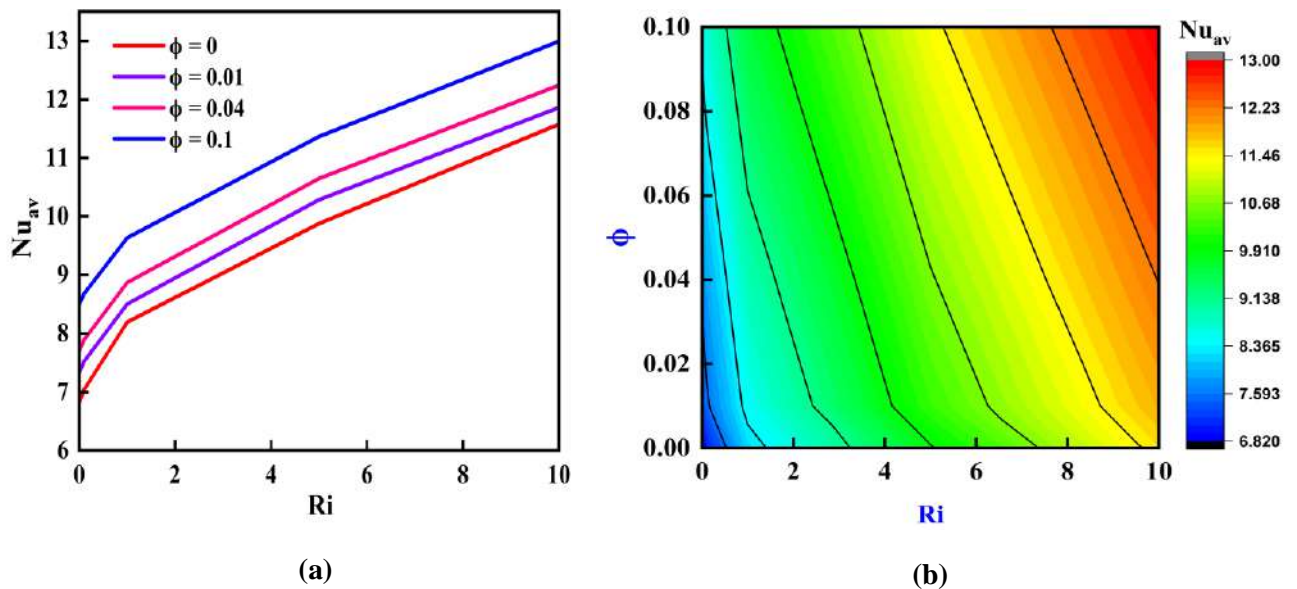
Figure 3.11: Influence of ϕ and Ri on Nu_{av}: (a) 2D line graph; (b) 2D contour.

Actually, a remarkable modification in heat transportation happens from the hot surface to the cold one due to the presence or absence of nanoparticles. The H_2O-TiO_2 nanofluid shows superiors heat transport performance on the strength of extra-ordinary thermal characteristics of nanofluid. Though the magnetic field impose resistance to heat transfer, the nanofluid (H_2O-TiO_2) also exhibits more heat transfer performance than only for base fluid (H_2O) which is clear from the Figure 3.12(b). That is, it can be concluded that the heat transfer performance is boosted up due to adding of TiO_2 nanoparticles into base fluid.

(a)	(b)
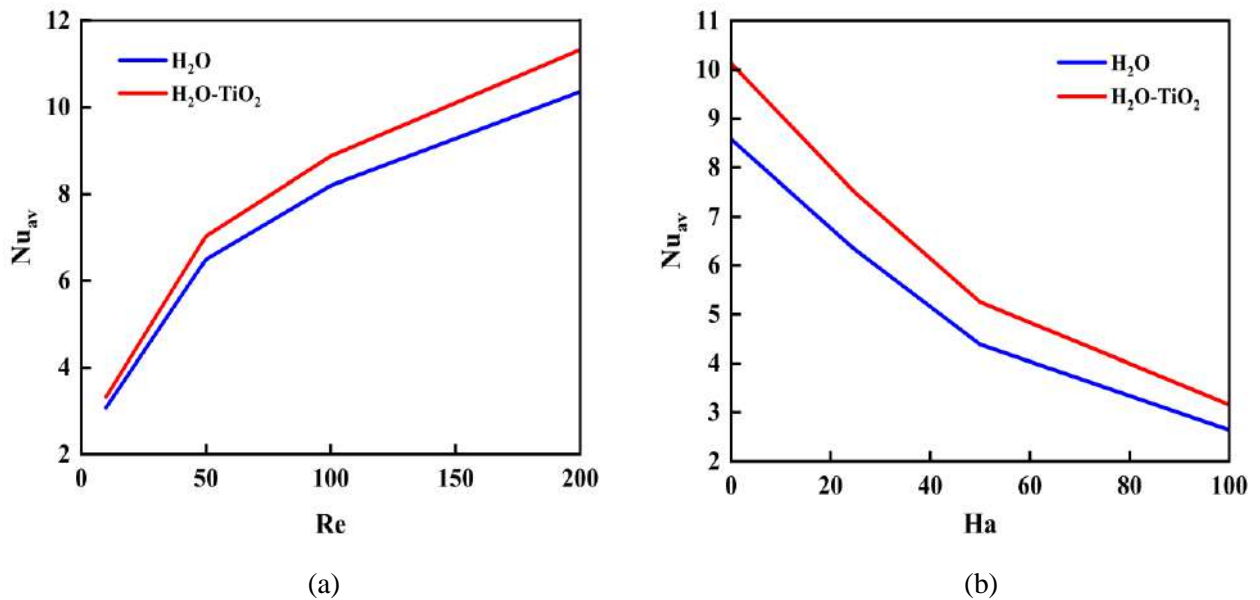
Figure 3.12: Variation of water and nanofluid on Nu_{av}: (a) with Re effect; (b) with Ha effect.

3.5 Response Surface Methodology

The statistical Response Surface Methodology (RSM) is used in this part to examine how the three key input parameters (Re, Ha and ϕ) affect the average Nusselt number (Nu_{av}) for this mixed convective heat exchanger model. It also included that how dependent and independent factors interacted each other [60]. RSM is one of the useful methods for modelling multivariate issues when the interest-generating responses are simultaneously impacted by the input variables, according to Montgomery [61]. Additionally, the RSM is employed to determine the parameters' ideal status in the computations of the research domain. The initial task in the majority of RSM situations is to establish an experimental and analytical approximation for the functional relationship between the design parameters (output and input variables). Despite the fact that there are other RSM models available, the

second-order RSM model that takes into account all linear, square, and interaction factors is typically sufficient to approximating the response. The quadratic polynomial model is provided by the following:

$$y = a_0 + \sum_{i=1}^{3} a_i x_i + \sum_{i=1}^{3} a_{ii} x_i^2 + \sum_{i=1}^{3} a_{ij} x_i x_j \tag{3.1}$$

where y is the response function (output), a_0 is the intercept and a_i is the linear regression coefficient of ith factor. Also, a_{ii} is the quadratic regression coefficient of ith factor, and a_{ij} is the interaction of ith and j^{th} factors. Here, the involved parameters Re, Ha and ϕ are used as input factors whereas Nu_{av} from the hot surface is considered as response faction (y). The goal is to build a proper correlation between the independent variables and the response function by optimizing the response of the variable y. In 1992, a central composite design (CCD), which was first suggested by Box and Wilson [62], was used to match the second-order model. It is currently the most popular category of designs for second-order model fitting. Also, in this test, the range of the input variables Re, Ha and ϕ are $10 \le \text{Re} \le 200, 0 \le Ha \le 100$ and $0 \le \phi \le 0.1$ respectively. Three degrees of selection are available for these parameters (low, medium, high). The statistical model is also defined by the number of parameters and their levels. For a 3-factor face-centered (FC) CCD design, there are in total 20 runs: 8 cube points, 6 center points in cube and 6 axial points). A physical representation of face-centered CCD design for three factors are described in Figure 3.13.
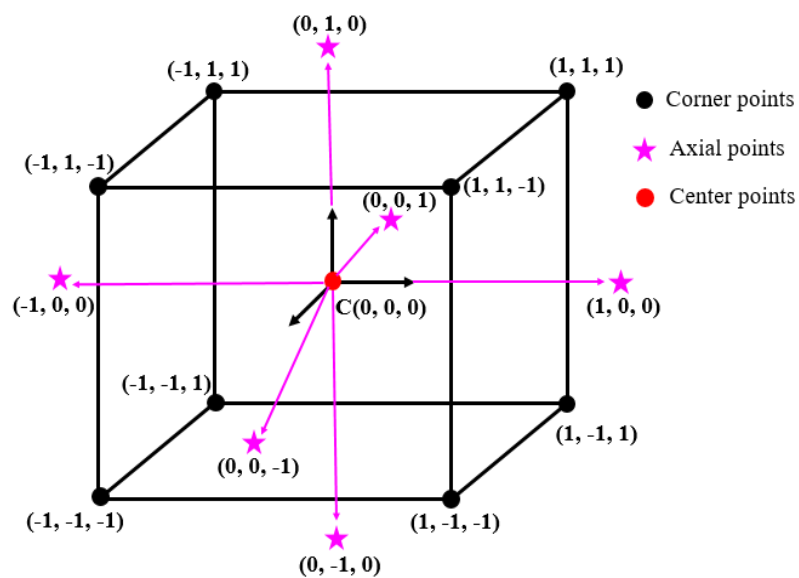
Figure 3.13: Schematic representation of a 3-factor FC-CCD design.

Table 5: Codded levels and design variables for CCD.

Variables Name (factors)	Coded Level		
	-1 (low)	0 (medium)	1 (high)
Re	10	105	200
Ha	0	50	100
ϕ	0	0.05	0.1

Table 6: Levels of input factors and response function.

Run Order	Codded Values			Real Values			Response
	Re	Ha	ϕ	Re	Ha	ϕ	Nu_{av}
1	0	0	0	105	50	0.05	3.7066
2	-1	0	0	10	50	0.05	2.3517
3	0	0	0	105	50	0.05	3.7066
4	0	-1	0	105	0	0.05	7.9067
5	0	1	0	105	100	0.05	2.7937
6	0	0	0	105	50	0.05	3.7066
7	-1	-1	-1	10	0	0	3.4744
8	0	0	1	105	50	0.1	4.0539
9	1	1	-1	200	100	0	2.6479
10	-1	1	-1	10	100	0	1.9219
11	-1	-1	1	10	0	0.1	3.8395
12	1	1	1	200	100	0.1	3.2588
13	1	-1	1	200	0	0.1	9.264
14	0	0	-1	105	50	0	3.3928
15	-1	1	1	10	100	0.1	2.3659
16	0	0	0	105	50	0.05	3.7066
17	1	-1	-1	200	0	0	7.7847
18	0	0	0	105	50	0.05	3.7066
19	1	0	0	200	50	0.05	4.1984
20	0	0	0	105	50	0.05	3.7066

The codded levels of input variables for CCD are described in Table 5. Moreover, Table 6 displays the configurations of the simulation runs for both coded and real values based on the CCD. Using analytical software, the quadratic polynomial regression equations are statistically analyzed, and the corresponding coefficients and the effects of the parameters on variables are defined. After that, the experiment's design is used to examine the response and variables (as coded values). Using a specific coefficient of determination and change resources, depending on the p-value with a 95% certainty level, the fitting quality of the experiments' results has been accepted or rejected. Finally, analysis of variance (ANOVA), contour plot, 3D surface plot, and sensitivity analysis have all been used to assess the results.

3.6 Analysis of variance

This section performs investigation about estimated regression and statistical analysis of experimental models due to simulation studies that are taken into account under various experimental substances. Figure 3.14 displays three different residual plots that are produced after entering the data into analytical software and doing a variance analysis (ANOVA). The goodness-of-fit in regression is examined using graphs called residual plots. The normal probability plots of the residuals are in good shape when taking into account Figure 3.14(a).

The normal probability plots of the residual distributions are actually shown in order to examine the normality of the observation. Due to the fact that this line is straight, it is assumed that the residual distribution for Nu_{av} is normal. A good correlation between the observed and fitted values can be seen in Figure 3.14(b) by contrasting the residual diagrams and fitted values [63]. The variances of the error terms are comparable because the residuals generally form a horizontal band around the zero line. All responses show a range of residuals, with the greatest residuals being close to 0.6. Moreover, the distribution of residual histograms in Figure 3.14(c) is skewed and does not resemble a symmetrical distribution. Also, it is noteworthy that none of the residuals deviate significantly from the fundamental random pattern of residuals, suggesting that there are no outliers. The residuals for Nu_{av} clearly bounce around the zero line arbitrarily, indicating that they are uncorrelated with one another. So, it can be said that the current RSM model has a respectable level of accuracy.
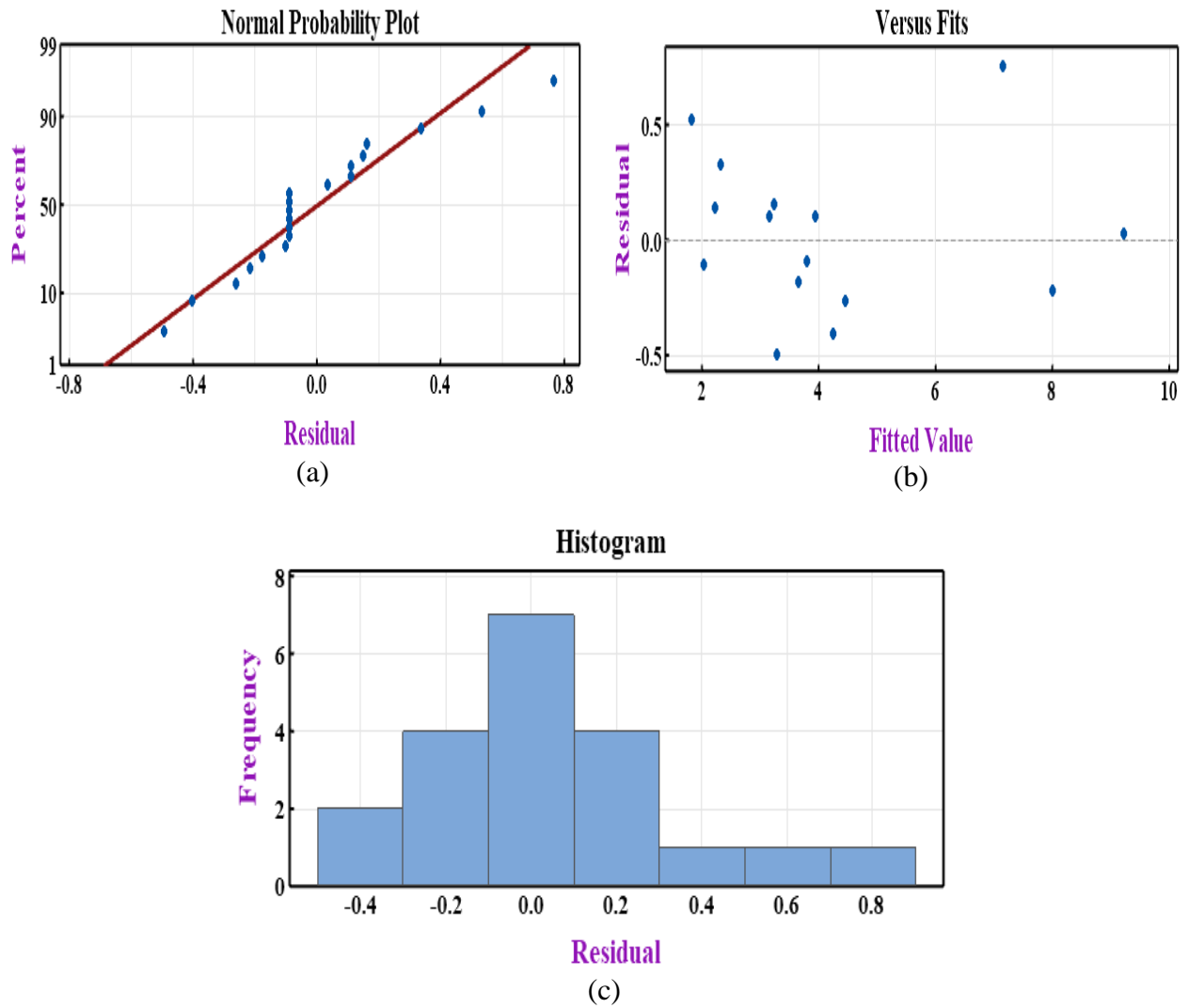
Figure 3.14: Residual plots for response function Nu_{av}: (a) normal probability plot; (b) residual vs fit value plot; (c) histogram of residual.

Moreover, the findings of the statistical analysis for this heat exchanger model by using RSM are shown in Table 7-8. According to Tables 7, the degrees of freedom (DOF) represent the maximum number of independent terms in this model. The total sum of squares (SS) is a tool for expressing the overall variation due to several causes. The value of Adj. SS (represents the adjusted sums of squares) is 70.2924 which is quite significant. The F-value, which is equal to 47.05 and does not result from noise, expresses that the Nu_{av} model is statistically significant. Here, the p-value is a very significant indicator of this statistical analysis, where p-value denotes the likelihood that the null hypothesis will be correct for a specific statistical model. In general, the p-value, which ranges from 0 to 1, is used to describe the statistical significance level. The null hypothesis is rejected when the p-value is very small ($0 < $ p-value $ < 0.01$) since it indicates stronger evidence that the result is

strongly statistically significant. Again, the range 0.01 < p-value ≤ 0.05 also indicates statistically significant. But the range p-value > 0.05 indicates don't reject the null hypothesis because this result is not statistically significant. From Table 7, it is notable that these input factors are significant for this model.

Table 7: Analysis of variance (ANOVA) for Nu_{av}.

Source	DOF	SS	Adj. SS	Adj. MS	F-value	p-value	Comment
Model	9	70.29	70.2924	7.8103	47.05	<0.0001	**Significant**
Linear	3	55.88	55.8688	18.6229	112.2	-	
Re	1	17.43	17.4251	17.4251	104.98	<0.0001	
Ha	1	37.18	37.1761	37.1761	223.97	<0.0001	
ϕ	1	1.27	1.2676	1.2676	7.64	0.02	
Square	3	6.838	5.9071	1.969	11.86	-	
Re*Re	1	1.18	1.1815	1.1815	7.12	0.0236	
Ha*Ha	1	5.54	5.5427	5.5427	33.39	0.0002	
$\phi * \phi$	1	0.1180	0.118	0.118	0.71	**0.4188**	
Interaction	3	8.5131	8.5165	2.8388	17.1	-	
Re*Ha	1	8.23	8.2335	8.2335	49.6	<0.0001	
Re* ϕ	1	0.2052	0.2052	0.2052	1.24	0.02923	
Ha* ϕ	1	0.0779	0.0779	0.0779	0.47	**0.5088**	
Residual Error	10	1.66	1.6598	0.166	-	-	
Lack-of-Fit	5	1.66	1.6598	0.332	-	-	**Insignificant**
Pure Error	5	0.000	0.000	0.000	-	-	
Total	19	71.95	71.9522				

*Here, **R^2 = 97.69%**, **Adjusted R^2 = 95.62%**, **Predicted R^2 = 80.84%**

Also, the statistical analysis of the model and testing procedures suggest high values of the R^2 (97.69%) for Nu_{av}, demonstrating that this model is suitable for computing the values of the response function Nu_{av}. The adjusted R^2 (95.62%) is less than the R^2 (97.69%) for Nu_{av}, yet the model still adequately matches the experimental data [64]. Another key indicator is Lack-of-Fit, which is needed very low for an appropriate model. It is noted that, there are different order (linear, quadratic, cubic, quadratic vs 2FI, cubic vs 3FI, etc.) model for RSM model. But, by observing all the significant values, the Table 8 and Table 9 say that the 'Quadratic vs 2FI' (2FI: 2-factors interaction) model is the best than any others.

Table 8: Fit summery statistics for Nu_{av}.

Source	Sum of Squares	Mean Square	F-value	p-value	
Mean vs Total	332.06	332.06	-	-	
Linear vs Mean	55.87	18.62	18.53	< 0.0001	
2FI vs Linear	8.52	2.84	4.88	0.0174	
Quadratic vs 2FI	**5.91**	**1.97**	**11.86**	**0.0012**	**Suggested**
Cubic vs Quadratic	1.49	0.3736	13.55	0.0037	Aliased
Residual	0.1655	0.0276			
Total	404.02	20.20			

Table 9: Model summery statistics for Nu_{av}.

Source	Std. Dev.	R²	Adjusted R²	Predicted R²	
Linear	1.00	0.7765	0.7346	0.5655	
2FI	0.7629	0.8948	0.8463	0.7146	
Quadratic	**0.4074**	**0.9769**	**0.9562**	**0.8048**	**Suggested**
Cubic	0.1661	0.9977	0.9927	-1.8254	Aliased

3.7 Regression Model Estimation

The following are the general models that the RSM produced for analyzing the relationship between the response (Nu_{av}) and the effective input parameters (Re, Ha, and ϕ):

$$y = a_0 + a_1\,Re + a_2\,Ha + a_3\,\phi + a_{11}\,Re^2 + a_{22}\,Ha^2 + a_{33}\,\phi^2 + a_{12}\,Re\,Ha$$
$$+ a_{13}\,Re\,\phi + a_{23}\,Ha\,\phi \tag{3.2}$$

where $a_0, a_1, a_2, a_3, a_{11}, a_{22}, a_{33}, a_{12}, a_{13}$, and a_{23} are coefficients of the best fitted regression model for this RSM model about the input factors Re, Ha, and ϕ. The Table 10 shows the estimated coefficients of equation (3.2) for Nu_{av}, which are derived as coded units. It is notable that only the important model terms which have low p-value (≤ 0.05) have been taken to build a proper regression equation due to the significance of these terms. Conversely, while the meaningless terms have been ignored (bold marked).

That is, the term *Re*, *Ha*, ϕ, *Re*^{2}, *Ha*^{2}, *Re.Ha*, and *Re.ϕ* are significant term for the response function average Nusselt number (*Nu*$_{av}$).

Table 10: Predictable regression coefficients for *Nu*$_{av}$ from RSM.

Coefficients	Actual Values	p-Values
a_0	3.278	-
a_1	0.03814	<0.0001
a_2	-0.071	<0.0001
a_3	0.138	0.02
a_{11}	-0.000073	0.0236
a_{22}	0.000568	0.0002
a_{33}	-82.9	**0.4188**
a_{12}	-0.00021	<0.0001
a_{13}	0.0337	0.02923
a_{23}	-0.0395	**0.5088**

Conversely, the term ϕ^2 and *Ha.ϕ* are totally insignificant for *Nu*$_{av}$ that must be omitted to final best fitted regression model. So, the following mathematical connection can be used to summarize the relationship between the response function (*Nu*$_{av}$) and the input variables (*Re*, *Ha*, and ϕ):

$$Nu_{av} = 3.278 + 0.03814\,\mathrm{Re} - 0.071\,Ha + 0.138\,\phi - 0.000073\,\mathrm{Re}^2$$
$$+ 0.000568\,Ha^2 - 0.000214\,\mathrm{Re}\,Ha + 0.0337\,\mathrm{Re}\,\phi \tag{3.3}$$

3.8 Response Surface Analysis

In this section, 2D and 3D response surface contour plots receiving from RSM have been provided in Figures 3.15-3.20 to examine the effects of effective parameters on the response function (Nu_{av}). The Figure 3.15 represents the effect of the factors Re and Ha on the response function. It is clear from this 2D contour plot that raising Re while lowering Ha raises the average Nusselt number while the another factor ϕ (0.1) remain fixed. At $Re =$ 200 and $Ha = 0$, the Nu_{av} is at its highest, whereas at $Re = 10$ and $Ha = 100$, it is at its lowest. Moreover, a 3D surface plot is represented by the Figure 3.16 for observing the effects of Re and Ha on Nu_{av}.

Figure 3.15: Variation of Nu_{av} for significant parameters Re and Ha: 2D view.
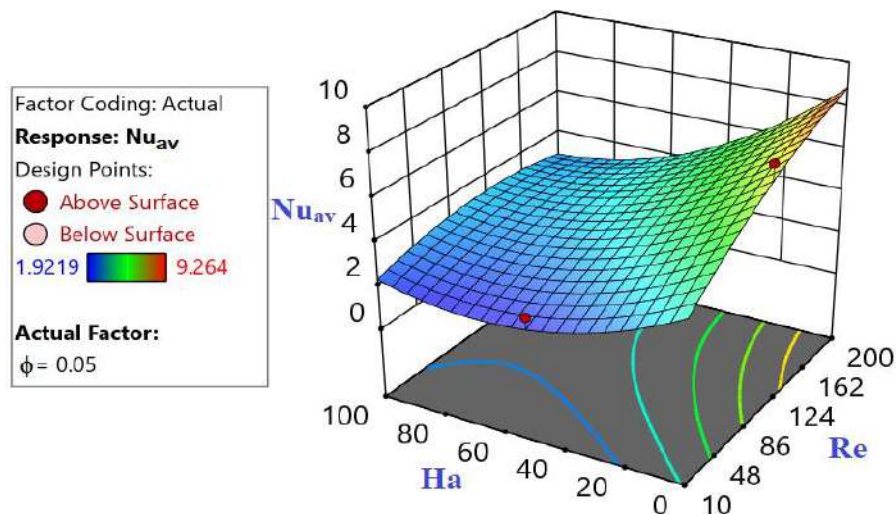
Figure 3.16: Variation of Nu_{av} for significant parameters Re and Ha: 3D view.

These two response surface plot exhibit the same behavior on the response function. Once more, the Figure 3.17 shows the fluctuations of response function Nu_{av} with Re and ϕ. The Nu_{av} increases when both Re and ϕ are improved by keeping another factor ($Ha = 10$) fixed. At $Re = 200$ and $\phi = 0.1$, the Nu_{av} is at its highest, whereas at $Re = 10$ and $\phi = 0$, it is at its lowest level. Furthermore, another 3D surface plot is represented by the Figure 3.18 for observing the effects of Re and ϕ on Nu_{av}, whereas these two response surface plot demonstration the same behavior on the response function Nu_{av}.
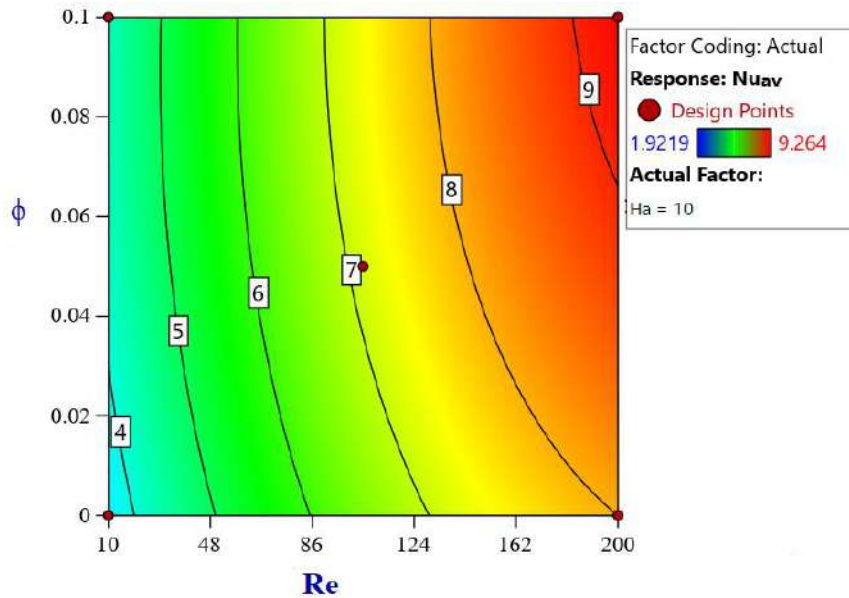
Figure 3.17: Variation of Nu_{av} for significant parameters Re and ϕ: 2D view.
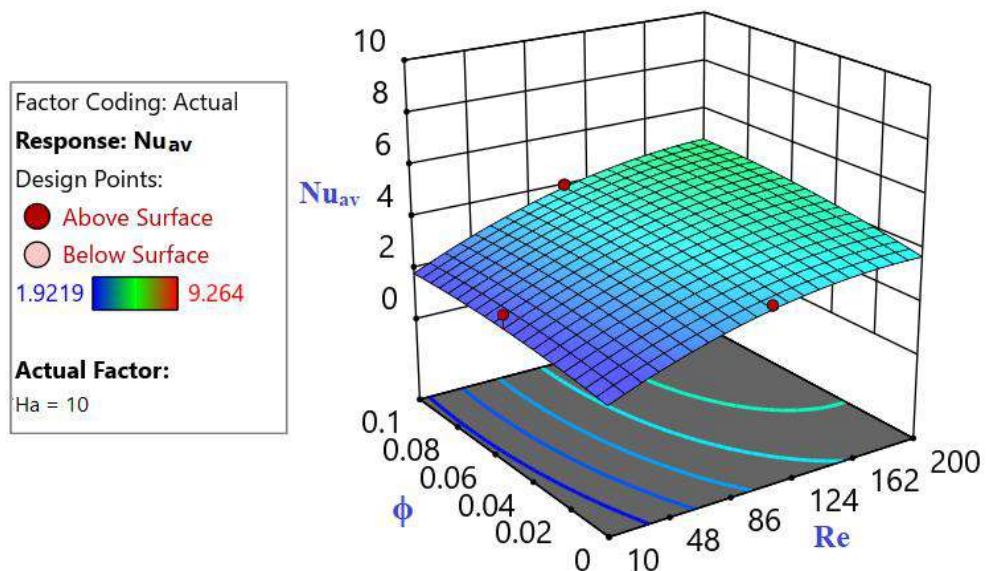
Figure 3.18: Variation of Nu_{av} for significant parameter Re and ϕ: 3D view.

Similarly, another 2D graphical illustrates is expressed by Figure 3.19 to describe how a decrease in *Ha* and an increase in ϕ result in an upsurge in the response function *Nu_av*. In that time, the value of another factor remains holds (*Re* = 100). The *Nu_av* is the greatest when $\phi = 0.1$ and *Ha* = 0, and it is lowest when $\phi = 0$ and *Ha* = 100. Also, the Figure 3.20 represents the control of *Ha* and ϕ on response function in 3D view.
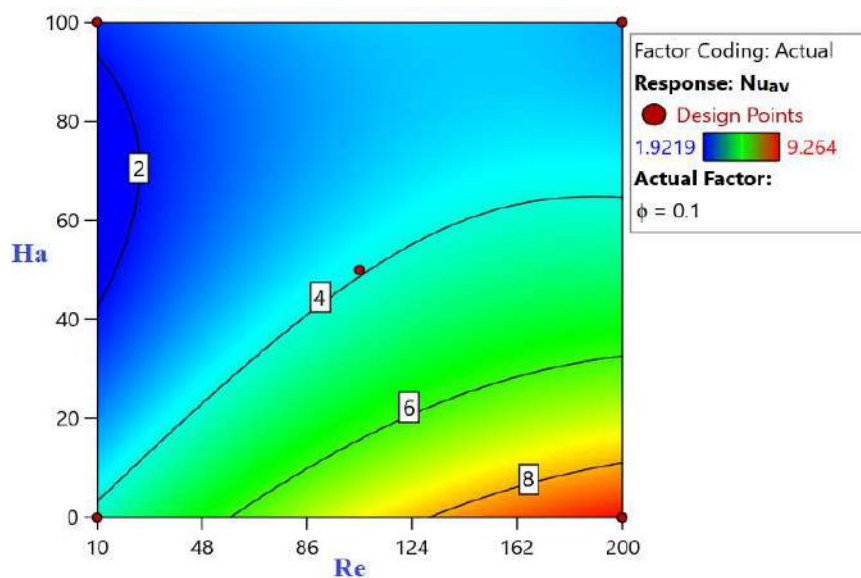

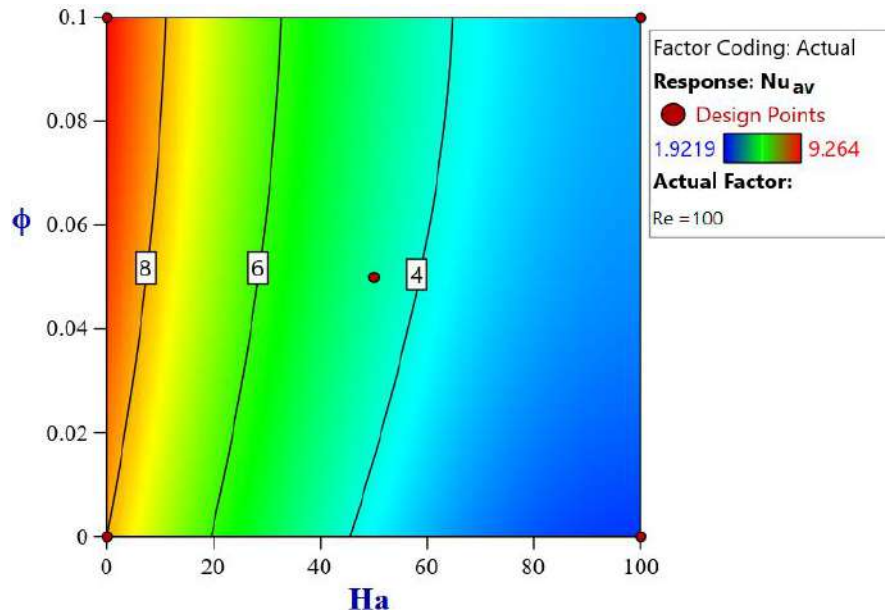**Figure 3.19:** Variation of *Nu_av* for significant parameters *Ha* and ϕ: 2D view.
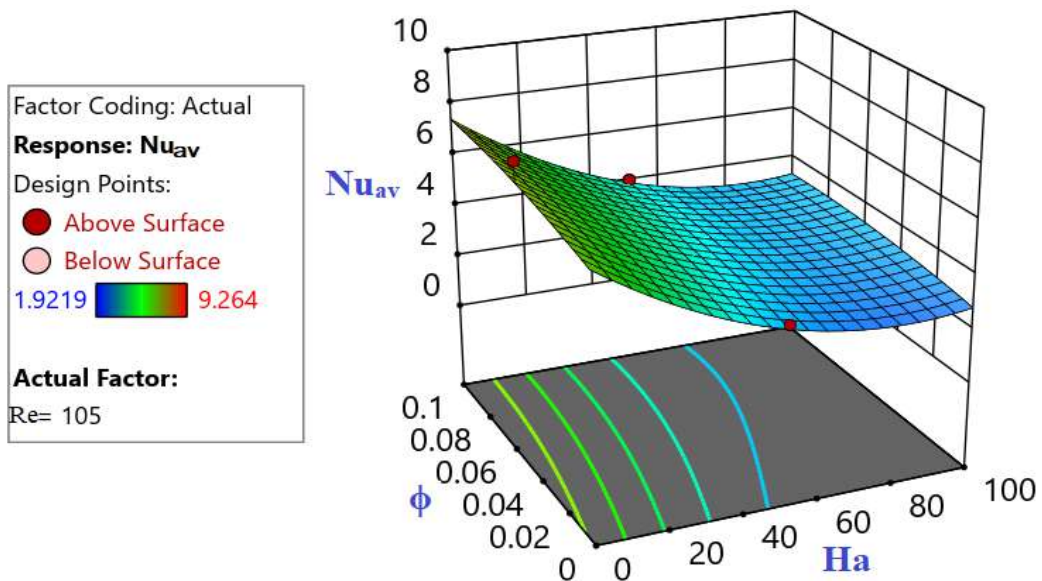

Figure 3.20: Variation of *Nu_av* for significant parameter *Ha* and ϕ: 3D view.

63

3.9 Sensitivity Analysis

Numerical simulation heavily relies on sensitivity analysis, a technique for figuring out how the uncertainties in a model input affect the model output [65]. Also, the phrase "sensitivity analysis" refers to figuring out how the RSM model's input parameters affect its output variables. The most effective parameter can then be identified by using the sensitivity analysis results to rank the effective parameters according to their influence. The sensitivity analysis tests on mathematical and computational models are carried out in order to determine the sensitivity of the model outputs to the uncertainty of the parameter values, input variables, and calculations [66]. The most efficient parameters or input values on the model outputs are determined utilizing the findings of these experiments. The sensitivity of the output variables with regard to specific effective factors (Re, Ha and ϕ) is calculated mathematically using the partial derivatives of the response function Nu_{av}. As a result, the partial derivatives of equation (3.3) to the input parameters are computed and provided as follows:

$$\frac{\partial Nu_{av}}{\partial Re} = 0.03814 - 0.000146\,Re - 0.000214\,Ha + 0.0337\phi \tag{3.4}$$

$$\frac{\partial Nu_{av}}{\partial Ha} = -0.071 + 0.001136\,Ha - 0.000214\,Re \tag{3.5}$$

$$\frac{\partial Nu_{av}}{\partial \phi} = 0.138 + 0.0337\,Re \tag{3.6}$$

Now, the equations (3.4)-(3.6) can be used to compute the response function's (Nu_{av}) sensitivity results in relation to the input variables Re, Ha, and ϕ. The results are shown in Table 11. These values are obtained using the suggested mixed convective heat exchanger model with Re at coded levels of -1, 0, 1 (10, 105, 200), Ha at levels of 0, 1 (0, 100), and ϕ at coded levels of -1, 0, 1 (0, 0.05, 0.1). It should be noted that the parameter levels are chosen on the basis of the idea that the parameter ranges are broad enough to reflect the fundamental principles and properties of Nu_{av}'s sensitivity to useful input parameters. Moreover, it's important to remember that a positive sensitivity number means that raising the input parameters causes the output parameter to rise. That means, the Reynolds number (Re) and nanoparticle volume fraction (ϕ) have a positive impact on the average Nusselt number (Nu_{av}). With the rising of Re and ϕ, the Nu_{av} must be increased.

Table 11: Sensitivity analysis of Nu_{av}.

Re	Ha	ϕ	$\dfrac{\partial Nu_{av}}{\partial \mathrm{Re}}$	$\dfrac{\partial Nu_{av}}{\partial Ha}$	$\dfrac{\partial Nu_{av}}{\partial \phi}$
	0	-1	0.00458	-0.07078	0.1043
-1	0	0	0.03828	-0.07078	0.1043
	0	1	0.07198	-0.07078	0.1043
	0	-1	0.00444	-0.0710	0.1380
0	0	0	0.03814	-0.0710	0.1380
	0	1	0.07184	-0.0710	0.1380
	0	-1	0.00429	-0.07121	0.1717
1	0	0	0.03799	-0.07121	0.1717
	0	1	0.07169	-0.07121	0.1717
	1	-1	0.00437	-0.06965	0.1043
-1	1	0	0.03807	-0.06965	0.1043
	1	1	0.07177	-0.06965	0.1043
	1	-1	0.004226	-0.06986	0.1380
0	1	0	0.037926	-0.06986	0.1380
	1	1	0.07162	-0.06986	0.1380
	1	-1	0.00408	-0.07007	0.1717
1	1	0	0.03778	-0.07007	0.1717
	1	1	0.07148	-0.07007	0.1717

Conversely, a negative sensitivity number means that raising the input parameters causes the output parameter to down which is totally opposite behavior. That means, the Hartmann number (Ha) has a negative impact on Nu_{av}. So, with the increasing of Ha, the average heat transfer rate must be diminished consequently. As a result, the average Nusselt number is more sensitive to Re and ϕ, according to sensitivity comparisons. To construct a mixed convective heat exchanger model for potential heat transfer augmentation, researchers should therefore pay closer attention to the two parameters. Furthermore, the length of the bar diagram of Figure 3.21 and Figure 3.22 represent the value of sensitivity, where the upright bar denotes positive sensitivity and the inverted bar denotes the negative sensitivity about Nu_{av}.
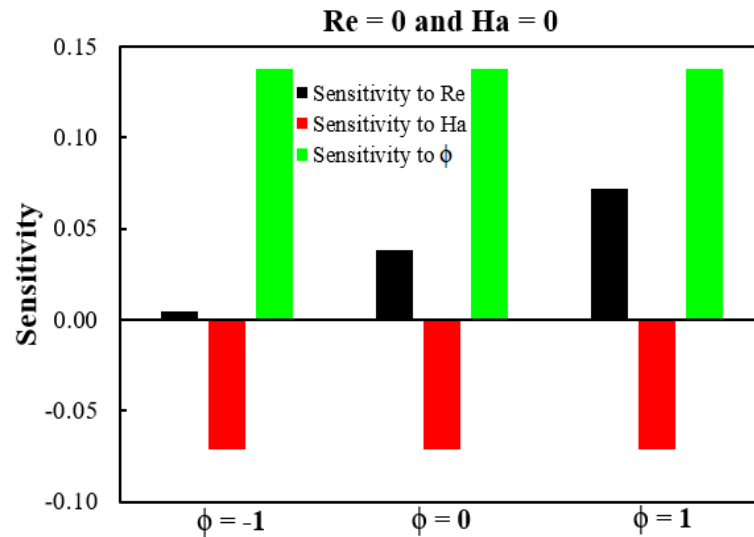
Figure 3.21: Sensitivity of Nu_{av} at $Re = 0$ and $Ha = 0$.
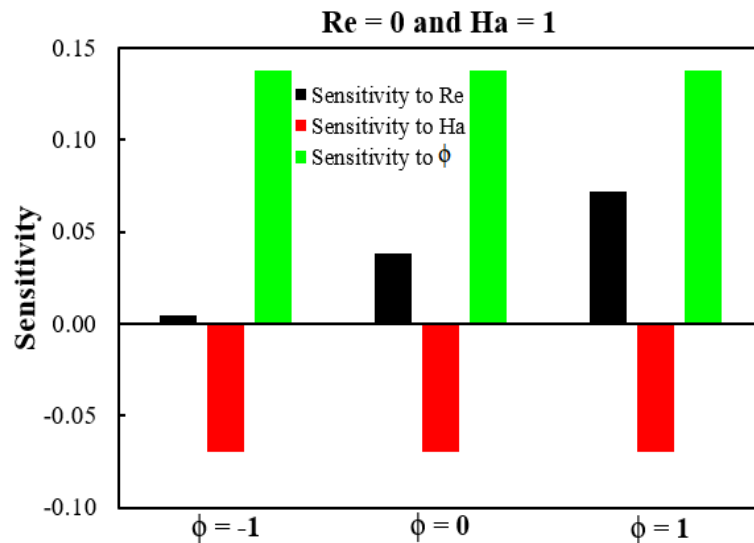
Figure 3.22: Sensitivity of Nu_{av} at $Re = 0$ and $Ha = 1$.

3.10 Optimization of Response Function

A multi-criteria methodology called RSM-based optimization, which has found widespread use in many engineering systems, allows for the simultaneous minimization and maximization of one or more responses [67]. The major goal of achieving an ideal heat transfer rate is to increase the system's energy efficiency and reduce associated costs. The objective of optimization in this section is to maximize the value of Nu_{av} in order to attain the highest heat transfer rate. Desirability or Derringer function, one of the most significant and widely used optimization methodologies, is applied to complete the optimization process utilizing CCD-RSM [68].

The maximum desirable value is chosen after the optimal solution is determined using the used numerical techniques. From the 55 possible optimal solution, the most 4 are given in Table 12 to get a clear description about the Nu_{av} optimization. In the end, it is determined that $Re = 200$, $Ha = 0$, and $\phi = 0.1$ with an acknowledged desirability of 0.999 are the ideal working conditions where the greatest heat transfer takes place.

Table 12: Optimization of response function Nu_{av}.

Run	Re	Ha	ϕ	Nu_{av}	Desirability	
1	**200**	**0**	**0.1**	**9.231**	**0.995**	**(Maximized)**
2	200	0	0.099	9.227	0.995	
3	199.25	0	0.1	9.221	0.994	
4	200	0	0.097	9.219	0.994	
5	200	0.002	0.096	9.211	0.993	
6	200	0	0.095	9.209	0.992	
7	199.997	0	0.095	9.206	0.992	
8	197.457	0	0.1	9.199	0.991	
9	200	0	0.092	9.194	0.990	
10	196.949	0.024	0.1	9.189	0.990	

CHAPTER 4

Conclusions and Recommendations

4.1 Summary of Major Outcomes

The present effort scrutinizes the dynamics of magnetized water conveying Titanium Oxide (Titania) nanomaterial subject to mixed convection in a hexagonal heat exchanger. Here, titanium oxide nanoparticles with spherical form are inserted in the water to create worked suspension. Streamline and isotherm line contours are depicted to describe the nanofluid flow domains for the crucial physical parameters like, Richardson number (Ri), Reynolds number (Re), Hartmann number (Ha), and nanoparticle volume fraction (ϕ). Followings are some of the key conclusions:

- The magnification in Reynolds number significantly strengthens the force convective heat transportation along the heat exchanger.

- A larger amount of Richardson number ($Ri =10$) indicates natural convective phenomena dominated where mixed convection occurs for only $Ri =1$.

- The average Nusselt number (Nu_{av}) becomes less sensitive to the Hartmann number and more sensitive to nanoparticle volume fraction (ϕ) when the Re number values are raised.

- In comparison to Re and Ha, in general, the heat transfer rate is more sensitive to the ϕ. Titania nanoparticle insertion augments water's ability to transmit heat.

- The ϕ and Ra have positive sensitivity on the average Nusselt number, but Ha has negative sensitivity.

- To establish an effective mixed convective hexagonal heat exchanger, the TiO_2-nanoparticle's size can be used up to 10%.

By including hybrid nanofluids, non-Newtonian flow models, various shaped geometrical enclosures, chemical reaction and radiation effects, the present flow model can be expanded. The thermal enactment of refrigerators, radiators, and microelectronic may be improved using the current findings.

4.2 Future Works

Future research in this field has a lot of potential because it has so many industrial and engineering applications. There are numerous additional mathematical representations for these nanofluids based heat exchanger model. As a result, there are several opportunities to broaden this inquiry. For the ongoing work on the current study, the following suggestions can be made:

❖ investigation about heat and mass transfer can be performed by using hybrid nanofluid involving distinct nanoparticles and base fluids.

❖ different physics, such as radiation effects, internal heat generation and absorption, and capillary effects might be incorporated to future study.

❖ the governing equation of concentration conservation can be used to study double diffusive mixed convection.

❖ a porous media can be used for further investigation to analyze the heat and mass transfer effect.

❖ different fluids or nanofluid, various thermal boundary conditions such as constant heat flux or radiation, and unsteady flow can all be used to extend the research to turbulent flow.

❖ in order to study the impact of involved factors on flow fields and heat transfer in cavities, this discussion may be expanded to include three-dimensional analyses.

❖ to study the heat transfer performance by using variable thermophysical properties.

References:

[1] Abdulmajeed, B. A., Hamadullah, S., and Allawi, F. A., "Deep oxidative desulfurization of model fuels by prepared nano TiO_2 with phosphotungstic acid," Journal of Engineering, vol. 24, pp. 41-52, 2018.

[2] Sheikholeslami, M., Said, Z., and Jafaryar, M., "Hydrothermal analysis for a parabolic solar unit with wavy absorber pipe and nanofluid," Renewable Energy, vol. 188, pp. 922-932, 2022.

[3] Hayat, T., Aziz, A., and Alsaedi, A., "Analysis of entropy production and activation energy in hydromagnetic rotating flow of nanoliquid with velocity slip and convective conditions," Journal of Thermal Analysis and Calorimetry, vol. 146 (6), pp. 2561-2576, 2021.

[4] Öztop, H. F., Sakhrieh, A., Abu-Nada, E., and Al-Salem, K., "Mixed convection of MHD flow in nanofluid filled and partially heated wavy walled lid-driven enclosure," International Communications in Heat and Mass Transfer, vol. 86, pp. 42-51, 2017.

[5] Batool, S., Rasool, G., Alshammari, N., Khan, I., Kaneez, H., and Hamadneh, N., "Numerical analysis of heat and mass transfer in micropolar nanofluids flow through lid driven cavity: Finite volume approach," Case Studies in Thermal Engineering, vol. 37, 102233, 2022.

[6] Sheikholeslami, M., and Chamkha, A. J., "Flow and convective heat transfer of a ferro-nanofluid in a double-sided lid-driven cavity with a wavy wall in the presence of a variable magnetic field," Numerical Heat Transfer, Part A: Applications, vol. 69 (10), pp. 1186-1200, 2016.

[7] Choi, S. U., and Eastman, J. A., "Enhancing thermal conductivity of fluids with nanoparticles," Argonne National Lab. (ANL), Argonne, IL (United States), 1995.

[8] Sheikholeslami, M., Gorji-Bandpy, M., and Ganji, D. D., "Numerical investigation of MHD effects on Al_2O_3 water nanofluid flow and heat transfer in a semi-annulus enclosure using LBM," Energy, vol. 60, pp. 501-510, 2013.

[9] Rahman, M. M., Öztop, H. F., Ahsan, A., Saidur, R., Al-Salem, K., and Rahim, N. A., "Laminar mixed convection in inclined triangular enclosures filled with water based Cu nanofluid," Industrial and engineering chemistry research, vol. 51 (10), pp. 4090-4100, 2012.

[10]   Cimpean, D. S., Sheremet, M. A., and Pop, I., "Mixed convection of hybrid nanofluid in a porous trapezoidal chamber," International Communications in Heat and Mass Transfer, vol. 116, 104627, 2020.

[11]   Ghadikolaei, S. S., and Gholinia, M., "3D mixed convection MHD flow of GO-MoS_2 hybrid nanoparticles in H_2O-(CH_2OH) 2 hybrid base fluid under the effect of H_2 bond," International Communications in Heat and Mass Transfer, vol. 110, pp. 104371, 2020.

[12]   Patil, P. M., and Kulkarni, M., "Analysis of MHD mixed convection in a Ag-TiO_2 hybrid nanofluid flow past a slender cylinder," Chinese Journal of Physics, vol. 73, pp. 406-419, 2021.

[13]   Vaidya, H., Prasad, K. V., Tlili, I., Makinde, O. D., Rajashekhar, C., Khan, S. U., and Mahendra, D. L., "Mixed convective nanofluid flow over a nonlinearly stretched Riga plate," Case Studies in Thermal Engineering, vol. 24, 100828, 2021.

[14]   Hirpho, M., and Ibrahim, W., "Mixed Convection Heat Transfer of a Hybrid Nanofluid in a Trapezoidal Prism with an Adiabatic Circular Cylinder," Mathematical Problems in Engineering, vol. 2022, 8170224, 2022.

[15]   Sheikholeslami, M., "Numerical analysis of solar energy storage within a double pipe utilizing nanoparticles for expedition of melting," Solar Energy Materials and Solar Cells, vol. 245, 111856, 2022.

[16]   Chamkha, A. J., Nabwey, H. A., Abdelrahman, Z. M. A., and Rashad, A. M., "Mixed bioconvective flow over a wedge in porous media drenched with a nanofluid," Journal of Nanofluids, vol. 8 (8), pp. 1692-1703, 2019.

[17]   Tayebi, T., Öztop, H. F., and Chamkha, A. J., "Natural convection and entropy production in hybrid nanofluid filled-annular elliptical cavity with internal heat generation or absorption," Thermal Science and Engineering Progress, vol. 19, 100605, 2020.

[18]   Menni, Y., Chamkha, A. J., and Ameur, H., "Advances of nanofluids in heat exchangers-A review," Heat Transfer, vol. 49 (8), pp. 4321-4349, 2020.

[19]   Xiong, P. Y., Hamid, A., Iqbal, K., Irfan, M., and Khan, M., "Numerical simulation of mixed convection flow and heat transfer in the lid-driven triangular cavity with different obstacle configurations," International Communications in Heat and Mass Transfer, vol. 123, 105202, 2021.

[20]   Molla, M. M., and Yao, L. S., "Mixed convection of non-Newtonian fluids along a heated vertical flat plate," International journal of heat and mass transfer, vol. 52 (13-14), pp. 3266-3271, 2009.

[21]   Bég, O. A., Khan, M. S., Karim, I., Alam, M. M., and Ferdows, M., "Explicit numerical study of unsteady hydromagnetic mixed convective nanofluid flow from an exponentially stretching sheet in porous media," Applied Nanoscience, vol. 4 (8), vol. 943-957, 2014.

[22]   Hatami, M., Zhou, J., Geng, J., Song, D., and Jing, D., "Optimization of a lid-driven T-shaped porous cavity to improve the nanofluids mixed convection heat transfer," Journal of Molecular Liquids, vol. 231, pp. 620-631, 2017.

[23]   Alshare, A., Abderrahmane, A., Guedri, K., Younis, O., Fayz-Al-Asad, M., Ali, H. M., and Al-Kouz, W., "Hydrothermal and Entropy Investigation of Nanofluid Natural Convection in a Lid-Driven Cavity Concentric with an Elliptical Cavity with a Wavy Boundary Heated from Below," Nanomaterials, vol. 12 (9), pp. 1392, 2022.

[24]   Manchanda, M., and Gangawane, K. M., "Mixed convection in a two-sided lid-driven cavity containing heated triangular block for non-Newtonian power-law fluids," International Journal of Mechanical Sciences, vol. 144, pp. 235-248, 2018.

[25]   Gangawane, K. M., Öztop, H. F., and Ali, M. E., "Mixed convection in a lid-driven cavity containing triangular block with constant heat flux: Effect of location of block, International Journal of Mechanical Sciences," vol. 152, pp. 492-511, 2019.

[26]   Mondal, P., and Mahapatra, T. R., "MHD double-diffusive mixed convection and entropy generation of nanofluid in a trapezoidal cavity," International Journal of Mechanical Sciences, vol. 208, 106665, 2021.

[27]   Sheikholeslami, M., Gorji-Bandpy, M., Ganji, D. D., Soleimani, S., and Seyyedi, S. M., "Natural convection of nanofluids in an enclosure between a circular and a sinusoidal cylinder in the presence of magnetic field," International Communications in Heat and Mass Transfer, vol. 39 (9), pp. 1435-1443.

[28]   Shekaramiz, M., Fathi, S., Ataabadi, H. A., Kazemi-Varnamkhasti, H., and Toghraie, D., "MHD nanofluid free convection inside the wavy triangular cavity considering periodic temperature boundary condition and velocity slip mechanisms," International Journal of Thermal Sciences, vol. 170, 107179, 2021.

[29]   Selimefendigil, F., and Öztop, H. F., "Corrugated conductive partition effects on MHD free convection of CNT-water nanofluid in a cavity," International Journal of Heat and Mass Transfer, vol. 129, pp. 265-277, 2019.

[30]   Abderrahmane, A., Qasem, N. A., Younis, O., Marzouki, R., Mourad, A., Shah, N. A., and Chung, J. D., "MHD Hybrid Nanofluid Mixed Convection Heat Transfer and Entropy Generation in a 3-D Triangular Porous Cavity with Zigzag Wall and Rotating Cylinder," Mathematics, vol. 10 (5), 769, 2022.

[31]   Alsedais, N., Aly, A. M., and Mansour, M. A., "Local thermal non-equilibrium condition on mixed convection of a nanofluid-filled undulating cavity containing obstacle and saturated by porous media," Ain Shams Engineering Journal, vol. 13 (2), 101562, 2022.

[32]   Parveen, N., and Alim, M. A., "MHD free convection flow with temperature dependent thermal conductivity in presence of heat absorption along a vertical wavy surface," Procedia Engineering, vol. 56, pp. 68-75, 2013.

[33]   Sheikholeslami, M., Hayat, T., and Alsaedi, A., "MHD free convection of Al_2O_3–water nanofluid considering thermal radiation: a numerical study," International Journal of Heat and Mass Transfer, vol. 96, pp. 513-524, 2016.

[34]   Parveen, N., and Alim, M. A., "Natural convection of fluid with variable viscosity and viscous dissipation from a heated vertical wavy surface in presence of magnetic field," Journal of Naval Architecture and Marine Engineering, vol. 17 (2), pp. 101-113, 2020.

[35]   Chamkha, A. J., and Aly, A. M., "MHD free convection flow of a nanofluid past a vertical plate in the presence of heat generation or absorption effects," Chemical Engineering Communications, vol. 198 (3), pp. 425-441, 2010.

[36]   Molla, M. M., Saha, S., and Hossain, M., "The effect of temperature dependent viscosity on MHD natural convection flow from an isothermal sphere," Journal of Applied Fluid Mechanics, vol. 5 (2), pp. 25-31, 2012.

[37]   Islam, T., Alam, M., Asjad, M. I., Parveen, N., and Chu, Y. M., "Heatline visualization of MHD natural convection heat transfer of nanofluid in a prismatic enclosure," Scientific Reports, vol. 11 (1), pp. 1-18, 2021.

[38]   Ali, M. M., Akhter, R., and Miah, M. M., "Hydromagnetic mixed convective flow in a horizontal channel equipped with Cu-water nanofluid and alternated baffles," International Journal of Thermofluids, vol. 12, 100118, 2021.

[39]   Jakeer, S., Reddy, P. B., Rashad, A. M., and Nabwey, H. A., "Impact of heated obstacle position on magneto-hybrid nanofluid flow in a lid-driven porous cavity with Cattaneo-Christov heat flux pattern," Alexandria Engineering Journal, vol. 60 (1), pp. 821-835, 2021.

[40] Ali, M. M., Akhter, R., and Alim, M. A., "Magneto-mixed convection in a lid driven partially heated cavity equipped with nanofluid and rotating flat plate," Alexandria Engineering Journal, vol. 61 (1), pp. 257-278, 2022.

[41] Haq, R. U., Soomro, F. A., Wang, X., and Tlili, I., "Partially heated lid-driven flow in a hexagonal cavity with inner circular obstacle via FEM," International Communications in Heat and Mass Transfer, vol. 117, 104732, 2020.

[42] Toudja, N., Labsi, N., Benkahla, Y. K., Ouyahia, S. E., and Benzema, M., "Thermosolutal mixed convection in a lid-driven irregular hexagon cavity filled with MWCNT–MgO (15-85%)/CMC non-Newtonian hybrid nanofluid," Journal of Thermal Analysis and Calorimetry, vol. 147, pp. 855-878, 2020.

[43] Rehman, K. U., Malik, M. Y., Al-Mdallal, Q. M., and Al-Kouz, W., "Heat transfer analysis on buoyantly convective non-Newtonian stream in a hexagonal enclosure rooted with T-Shaped flipper: hybrid meshed analysis," Case Studies in Thermal Engineering, vol. 21, 100725, 2020.

[44] Majeed, A. H., Mahmood, R., Shahzad, H., Pasha, A. A., Islam, N., and Rahman, M. M., "Numerical simulation of thermal flows and entropy generation of magnetized hybrid nanomaterials filled in a hexagonal cavity," Case Studies in Thermal Engineering, vol. 39, 102293, 2022.

[45] Fayz-Al-Asad, M., Sarker, M. M. A., and Munshi, M. J. H., "Numerical investigation of natural convection flow in a hexagonal enclosure having vertical fin," Journal of Scientific Research, vol. 11 (2), pp. 173-183, 2019.

[46] Garoosi, F., Hoseininejad, F., and Rashidi, M. M., "Numerical study of heat transfer performance of nanofluids in a heat exchanger," Applied Thermal Engineering, vol. 105, pp. 436-455, 2016.

[47] Plant, R. D., and Saghir, M. Z., "Numerical and experimental investigation of high concentration aqueous alumina nanofluids in a two and three channel heat exchanger," International Journal of Thermofluids, vol. 9, 100055, 2021.

[48] Islam, S., Bairagi, T., Islam, T., Rana, B. M. J., Reza-E-Rabbi, S. K., and Rahman, M. M., "Heatline visualization in hydromagnetic natural convection flow inside a prismatic heat exchanger using nanofluid," International Journal of Thermofluids, vol. 16, 100248, 2022.

[49]   Cao, Y., Ayed, H., Jarad, F., Togun, H., Alias, H., Issakhov, A., Dahari, M., Wae-hayee, M., and El Ouni, M. H., "MHD natural convection nanofluid flow in a heat exchanger: Effects of Brownian motion and thermophoresis for nanoparticles distribution," Case Studies in Thermal Engineering, vol. 28, 101394, 2021.

[50]   Zhang, C., Shi, S., Lu, Y., Qiang, Y., Wu, Y., and Ma, C., "Heat discharging and natural convection heat transfer performance of coil heat exchanger in single molten salt tank," Applied Thermal Engineering, vol. 166, 114689, 2020.

[51]   Basak, T., Roy, S., and Thirumalesha, C., "Finite element analysis of natural convection in a triangular enclosure: effects of various thermal boundary conditions," Chemical Engineering Science, vol. 62 (9), pp. 2623-2640, 2007.

[52]   Zienkiewicz, O. C., and Taylor, R. L., "The finite element method for solid and structural mechanics," Elsevier, 2005.

[53]   Reddy, J. N., "An Introduction to Nonlinear Finite Element Analysis Second Edition: with applications to heat transfer, fluid mechanics, and solid mechanics," OUP Oxford, 2014.

[54]   Shewchuk, J. R., "Delaunay refinement algorithms for triangular mesh generation. Computational geometry," vol. 22 (1-3), pp. 21-74, 2002.

[55]   Dechaumphai, P., and Kanjanakijkasem, W., "A finite element method for viscous incompressible thermal flows," Science Asia, vol. 25, pp. 165-172, 1999.

[56]   Brinkman, H. C., "The viscosity of concentrated suspensions and solutions," The Journal of chemical physics, vol. 20 (4), pp. 571-571, 1952.

[57]   Maxwell, J. C., "A treatise on electricity and magnetism," Oxford: Clarendon Press, vol. 1, 1873.

[58]   Sivakumar, V., Sivasankaran, S., Prakash, P., and Lee, J., "Effect of heating location and size on mixed convection in lid-driven cavities," Computers and Mathematics with Applications, vol. 59 (9), pp. 3053-3065, 2010.

[59]   Khanafer, K., and Aithal, S. M., "Mixed convection heat transfer in a lid-driven cavity with a rotating circular cylinder," International Communications in Heat and Mass Transfer, vol. 86, pp. 131-142, 2017.

[60]   Myers, R. H., Khuri, A. I., and Vining, G., "Response surface alternatives to the Taguchi robust parameter design approach," The American Statistician, vol. 46 (2), pp. 131-139, 1992.

[61]   Montgomery, D. C., "Design and analysis of experiments," John wiley and sons, 2017.

[62]   Box, G. E., and Wilson, K. B., "On the experimental attainment of optimum conditions," Breakthroughs in statistics: methodology and distribution, pp. 270-310, 1992.

[63]   Joardar, H., Das, N. S., and Sutradhar, G., "An experimental study of effect of process parameters in turning of LM6/SiCP metal matrix composite and its prediction using response surface methodology," International Journal of Engineering, Science and Technology, vol. 3 (8), pp. 132-141, 2011.

[64]   Shirvan, K. M., Mamourian, M., Mirzakhanlari, S., Öztop, H. F., and Abu-Hamdeh, N., "Numerical simulation and sensitivity analysis of effective parameters on heat transfer and homogeneity of Al_2O_3 nanofluid in a channel using DPM and RSM," Advanced Powder Technology, vol. 27 (5), pp. 1980-1991, 2016.

[65]   Saltelli, A., Ratto, M., Andres, T., Campolongo, F., Cariboni, J., Gatelli, D., and Tarantola, S., "Global sensitivity analysis: the primer," John Wiley and Sons, 2008.

[66]   Campolongo, F., and Braddock, R., "The use of graph theory in the sensitivity analysis of the model output: a second order screening method," Reliability Engineering and System Safety, vol. 64 (1), vol. 1-12, 1999.

[67]   Vahedi, S. M., Ghadi, A. Z., and Valipour, M. S., "Application of response surface methodology in the optimization of magneto-hydrodynamic flow around and through a porous circular cylinder," Journal of Mechanics, vol. 34 (5), pp. 695-710, 2018.

[68]   Rashidi, S., Bovand, M., and Esfahani, J. A., "Structural optimization of nanofluid flow around an equilateral triangular obstacle," Energy, vol. 88, pp. 385-398, 2015.